The Investigation of Tethered Satellite System Dynamics

Contract NAS8-36160

Quarterly Report #1

For the period 15 August 1984 through 30 November 1984

Principal Investigator

Dr. Enrico Lorenzini

November 1984

Smithsonian Institution
Astrophysical Observatory
Cambridge, Massachusetts 02138

The Smithsonian Astrophysical Observatory is a member of the Harvard-Smithsonian Center for Astrophysics

The Investigation of Tethered Satellite System Dynamics

Contract NAS8-36160

Quarterly Report #1

For the period 15 August 1984 through 30 November 1984

Principal Investigator

Dr. Enrico Lorenzini

Co-Investigators

Mr. David A. Arnold

Dr. Mario D. Grossi

Dr. Gordon E. Gullahorn

Summary

The studies carried out during the period from 15 August 1984 through 30 November 1984 are dealt with in this Quarterly Report. Such studies are related to the following areas of investigation:

a. The dynamic response of the TSS during the entire station-keeping phase for the first electrodynamic mission. From the simulations that we ran useful information such as the out-of-plane swing amplitude and the tether's bowing have been derived.

b. The dynamics of the slack tether. Our in-house high-resolution computer code, SLACK2, has been improved (additional work will be carried out in the future) both in capabilities and computational speed. A convincing test case has been run together with some fairly long simulations of a severed tether with variable longitudinal oscillation damping.

c. Safety hazard studies related to tether breakage or plasma contactor failure. Preliminary values of the potential difference after the failure and of the drop of the electric field along the tether axis have been computed.

d. The up-date of the satellite rotational dynamics model. Such up-date has been initiated but results are not yet available (they will be shown in the next Quarterly Report).

Figure Captions

Figure A, B, C
- In-Plane vs. Time (MKS Units)
- Out-of-Plane vs. Time (MKS Units)
- Current vs. Time (MKS Units)

(The current must be doubled to be consistent with the dynamic response.)
1st Case of TSS First Electrodynamic Mission. Station-Keeping Phase. No Damping.

Figure D, E, F
- In-Plane vs. Time (MKS Units)
- Out-of-Plane vs. Time (MKS Units)
- Current vs. Time (MKS Units)

(The current must be doubled to be consistent with the dynamic response.)
2nd Case of TSS First Electrodynamic Mission. Station-Keeping Phase. With Damping.

Figure G – Geometry for the Tether Bowing Analysis.

Figure H, I, J
- In-Plane Tether Bowing vs. Time (MKS Units)
- Out-of-Plane Tether Bowing vs. Time (MKS Units)
- Current vs. Time (MKS Units)

First Electrodynamic Mission. Average Current in the Tether= 0.85 Amp. The Pendular Libration has been removed from the plots to better show the tether deflection wrt. the Orbiter/Satellite line of sight.

Figure K-1 – The radial components vs. time for (a) a SKYHOOK run and (b) an equivalent SLACK2 run. See discussion in text.

Figure K-2 – Successive configuration plots for the case considered in text (the SKYHOOK results are shown).

Figure K-3 – The configuration plots for SKYHOOK and SLACK2 simulation of the same case (as discussed in text) are shown side by side for several values of T. SKYHOOK results are on the left, inverted to make the in-plane components agree.

Figure K-4 – Results from a SLACK2 run with a long tether remnant after break (20 kilometers remaining from 100 km tether; 30 segments in simulation). This demonstrates that a small randomization of the initial conditions allows successful simulation in long remnant cases. Configurations are shown at 50 second intervals for 2500 seconds.

Figure K-5 - SLACK2 results for a sequence of runs in which only the tether damping varies. Otherwise, the cases are all the same: 0.2 km remaining from a 20 km upward deployed tether; 35 segment discretization; 600 second simulation with output at 10 second intervals. Damping factors of 0%, 0.5%, 1% and 2% are used, as discussed in the text.

Figure K-6 - The final case of Figure K-5 (2% damping) is followed for 3000 seconds, showing configurations at 20 second intervals.

Figure L - Simplified equivalent circuit of electrodynamic tether.

Figure M - In-vacuo, elongated prolate spheroid model of long orbiting tether.

Figure N - Geometry for electric field computation.

Table of Contents

1.0 Introduction

This is the first quarterly report submitted by SAO under contract NAS8-36160, "The Investigation of Tethered Satellite System Dynamics," Dr. Enrico Lorenzini, PI, and covers the period from 15 August 1984 through 30 November 1984.

2.0 Technical Activity During Reporting Period and Program Status

2.1 TSS Tether Dynamics and Out-of-Plane Swing Amplitude During the Station-Keeping Phase of the First Electrodynamic Mission

2.1.1 Satellite Libration Dynamics

In order to determine the out-of-plane swing angle that can be expected in an electrodynamic mission, an integration lasting 80,000 seconds has been done for a case similar to what can be expected during the first flight. In the simulation a 100 metric ton Shuttle is at an altitude of 295 km with a 550 kg subsatellite deployed upward on a 20 km tether. Both the Shuttle and the subsatellite have plasma contactors and the resistance of the wire is 4000 ohms (value provided by MMA). Since the integration is a long one only two mass points have been used in the simulation. In this model the electrodynamic force is applied at the end of the wire instead of being distributed along the wire so that the torque causing librations of the tether is too large by a factor of two. The results can be scaled by multiplying the current by a factor of two to give physically meaningful results (further details on this point will be given later in this report).

The only properties of the wire modelled in the simulation are its stiffness and damping. The parameters for a 2 mm kevlar wire (the axial stiffness is supposed to be provided by the kevlar only) have been used which gives a stiffness of 10998 dynes/cm. A critical damping coefficient of 155122 dynes per cm/sec is used to suppress longitudinal vibrations that would cause slow numerical integration. Since the wire is stiff and no reel control algorithm is used, there is no damping of pendular oscillations. In the first run, the plasma contactors were modelled by using large balloon radii for the Shuttle and the subsatellite. This has the effect of grounding both ends of the wire to the plasma. The integration failed after about 15,000 seconds and the integration started taking very small integration steps. Electrodynamic integrations are difficult because of the very fast time constants of the electrodynamic variables. The model for charge collection by the balloon is non-linear and has discontinuities. A large balloon radius also makes the integration more critical. In order to make the integration easier, the balloon model was replaced by a one ohm resistor between the electrodes and the plasmas. This eliminates the non-linearity and discontinuities and accomplishes the objective of grounding the electrodes to the plasma.

The integration was started with the system on the x-axis at the ascending node headed Easterly (toward the +y axis) in a 28° inclination orbit. The epoch of the orbit was chosen so that the north magnetic pole is inclined toward the -y axis. In this orientation the orbit has an inclination of about 16.5° with respect to the magnetic equator. During the integration the poles rotates Easterly through almost one complete revolution. This rotation of the pole is the major factor affecting the electrodynamic force on the wire.

During the first half orbit (see Figure A, B and C), the in-plane libration angle reaches .6 km (1.7 deg) and the out-of-plane amplitude reaches .15 km (.4 deg). During the first 25,000 seconds the out-of-plane amplitude builds up to an amplitude of about .9 km (2.6 degrees) while the in-plane amplitude stays about the same. After 25,000 sec there is no significant change in the out-of-plane amplitude. The wire current averages about .85 amps over the run. This is equivalent to the torque of a current of 2 x .85 = 1.70 amps when the electrodynamic force is distributed along the wire instead of being applied to the end mass. By dividing the libration amplitude by a factor of two to suppress the overestimated torque, and by comparing it to the atmospheric mission case, it turns out that the out-of-plane angular momentum at the beginning of retrieval, for the first electrodynamic mission, is comparable to the one evaluated for the atmospheric mission (100 km tether and 0.2 deg out-of-plane angle). The build-up in the out-of-plane oscillation amplitude is the result of resonance between the electrodynamic driving force which has a resonant (small) component and the natural period of the out-of-plane oscillation which is at half the orbital period. The system can go off resonance because of a change in the period of either the driving force or the natural out-of-plane oscillation. The natural period lengthens with increasing amplitude, being exactly half the orbital period only for small amplitudes. The amplitude is still fairly small in this run, but the dependence of the period on amplitude has not been studied. Since the magnetic field is rotating with the earth, the change in the pole position may be a more likely cause of the system going off resonance.

ORIGINAL PAGE IS
OF POOR QUALITY

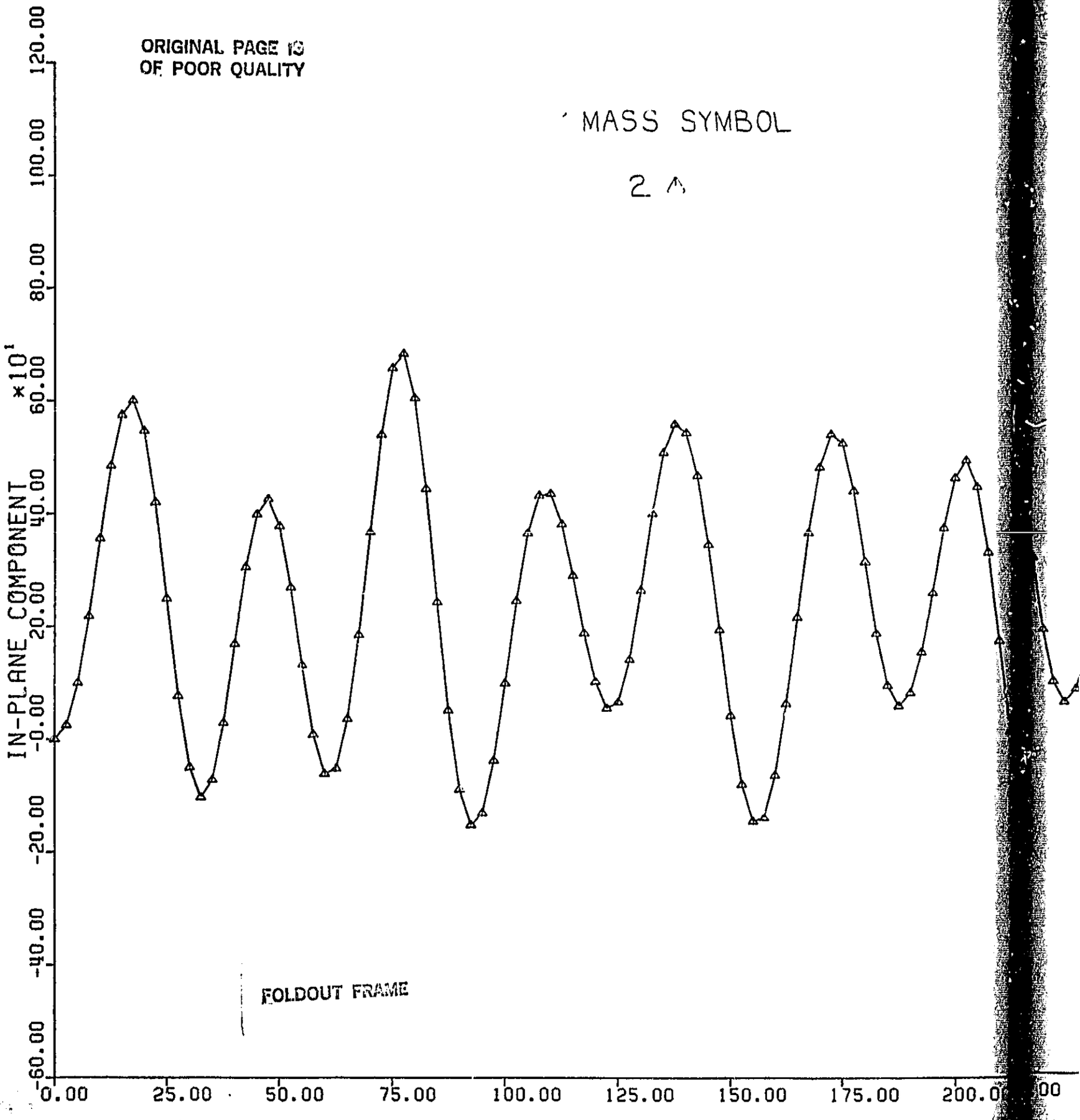

FOLDOUT FRAME

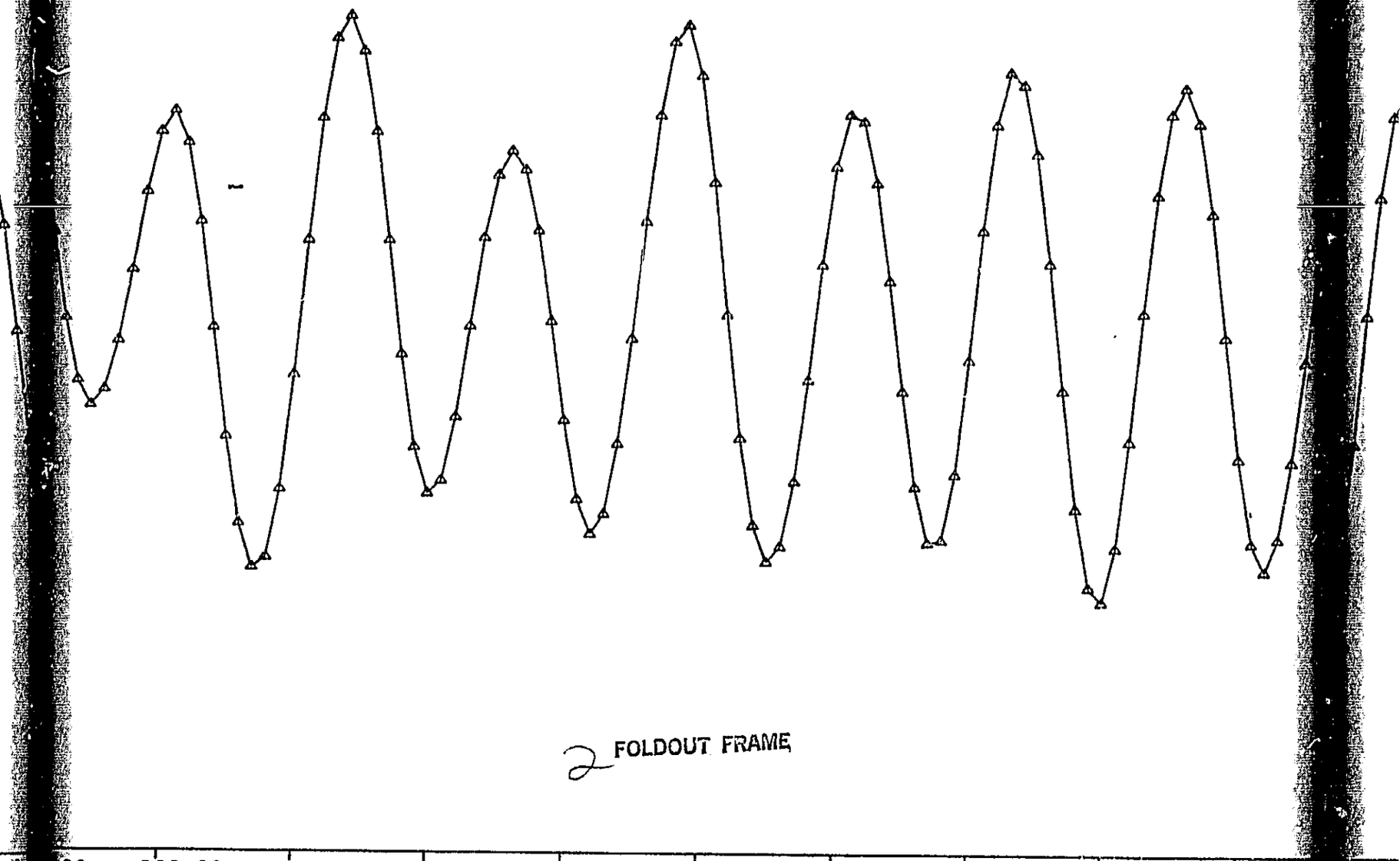

FOLDOUT FRAME 2

ORIGINAL PAGE IS
OF POOR QUALITY

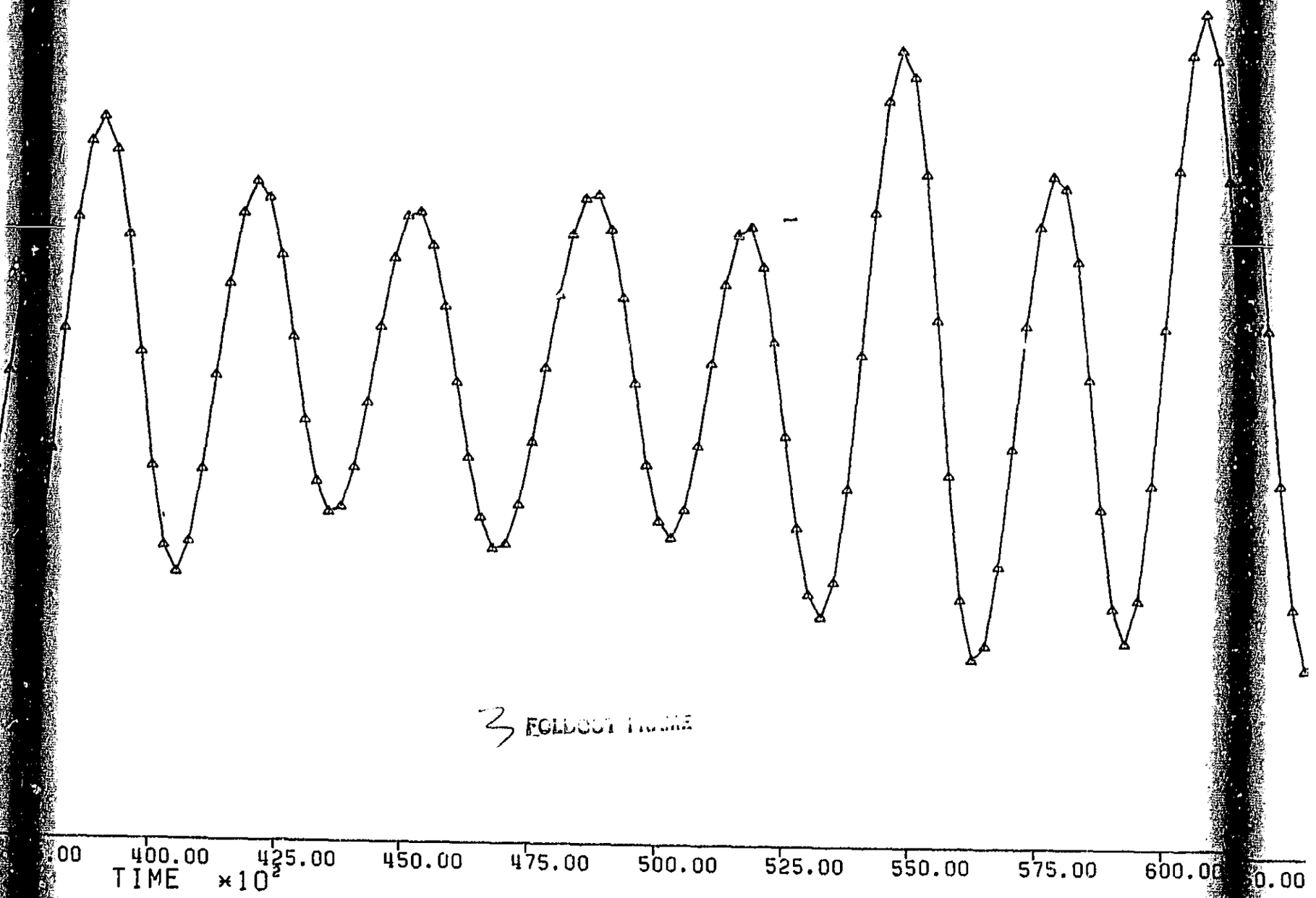

3 FOLLOUT FRAME

00 400.00 425.00 450.00 475.00 500.00 525.00 550.00 575.00 600.00 0.00

TIME $\times 10^2$

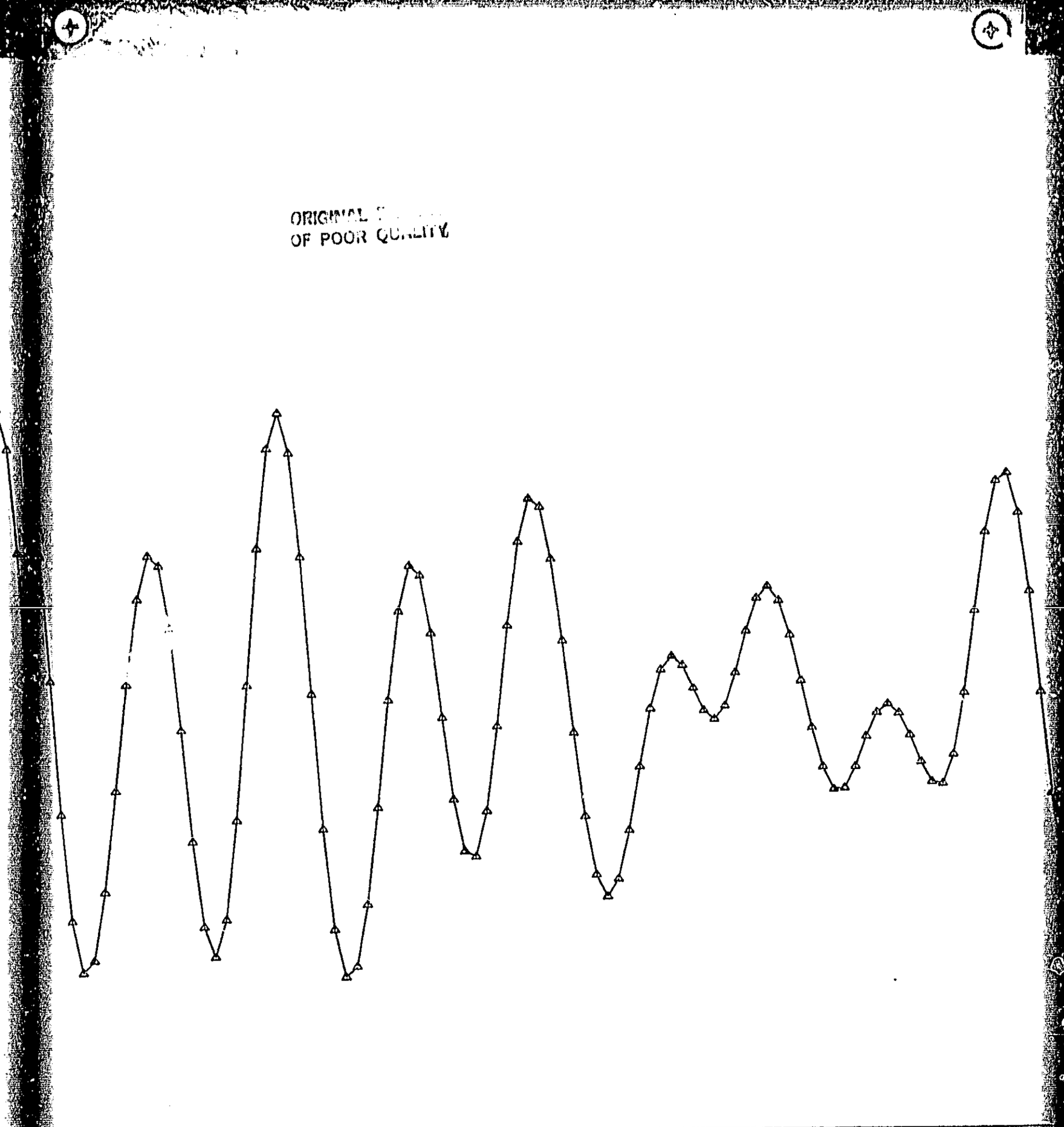

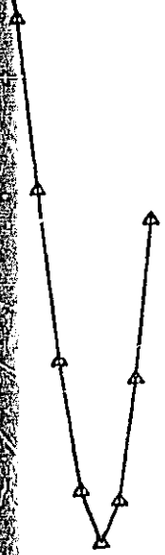

FOLDOUT FRAME 5

75.00 800.00

Figure A

MASS SYMBOL

2 4

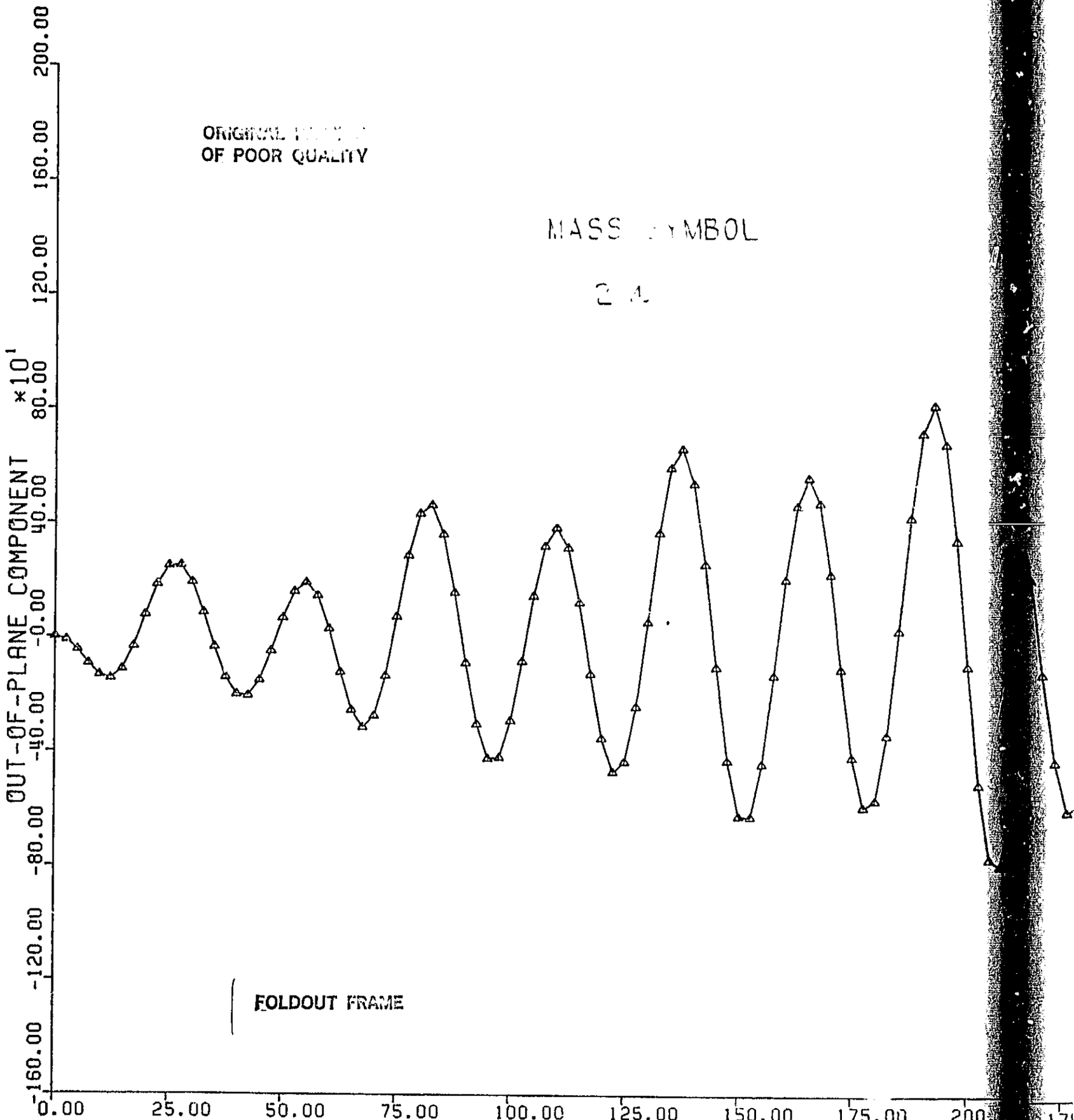

ORIGINAL PAGE IS
OF POOR QUALITY

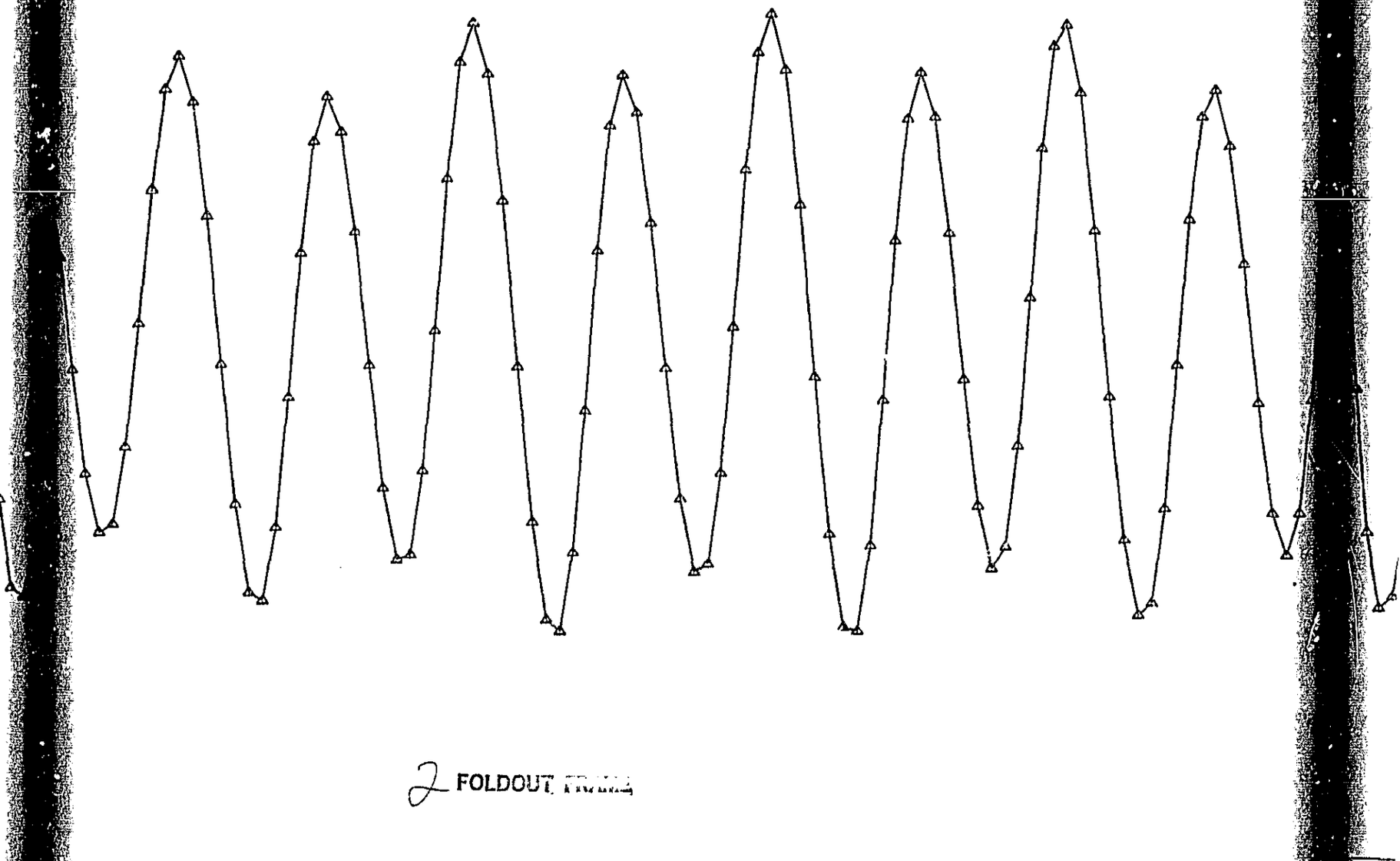

2 FOLDOUT FRAME

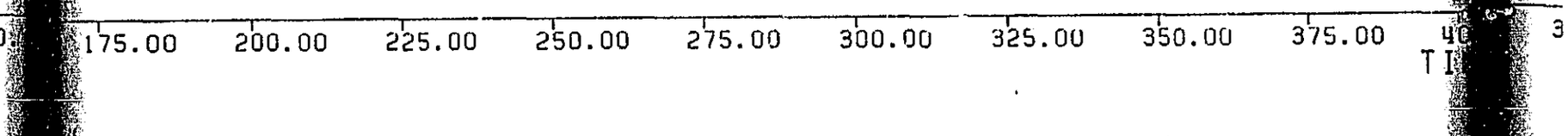

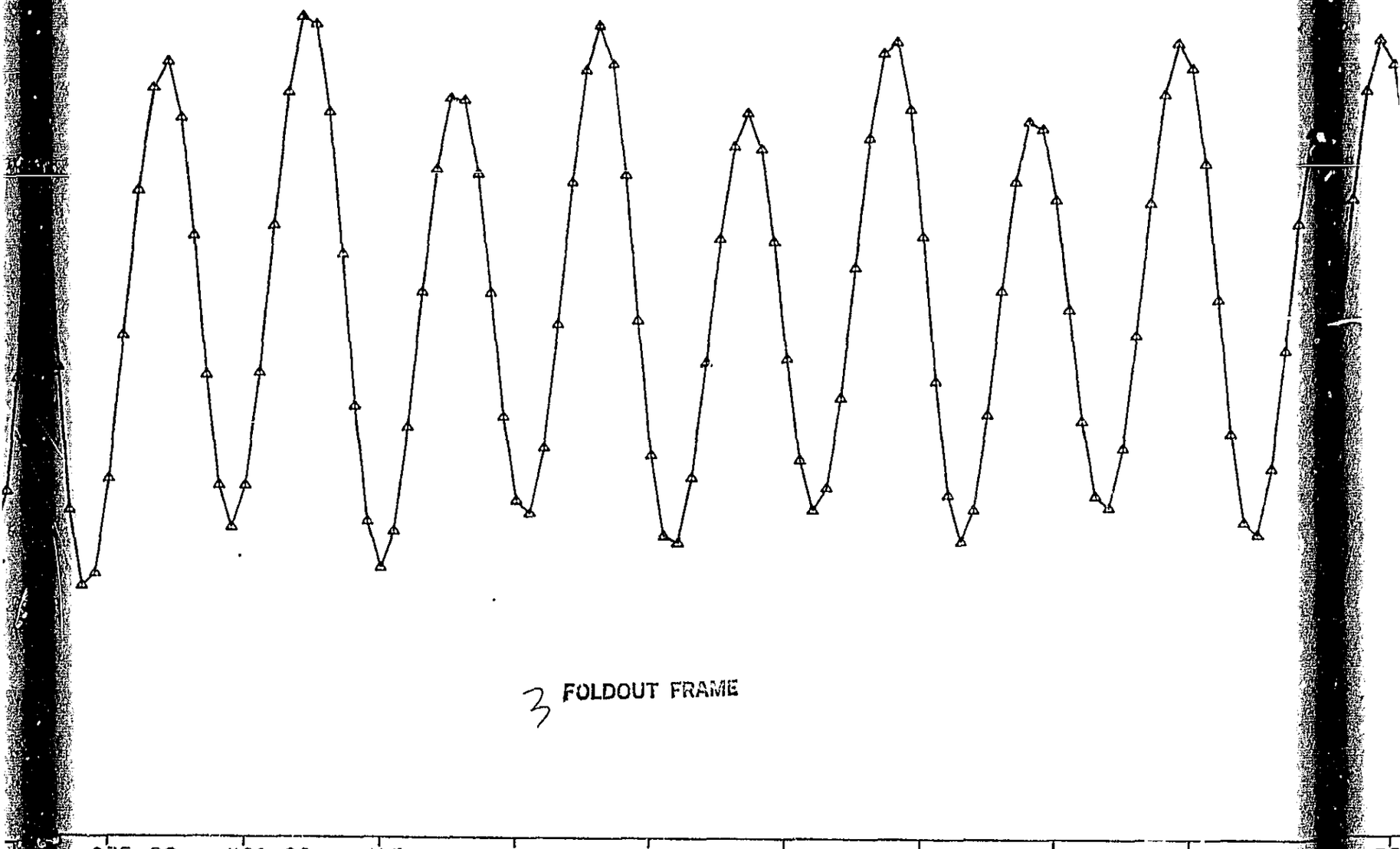

FOLDOUT FRAME 3

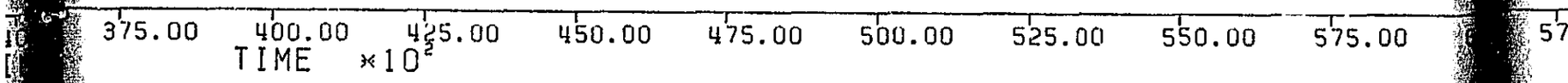

4 FOLDOUT FRAME

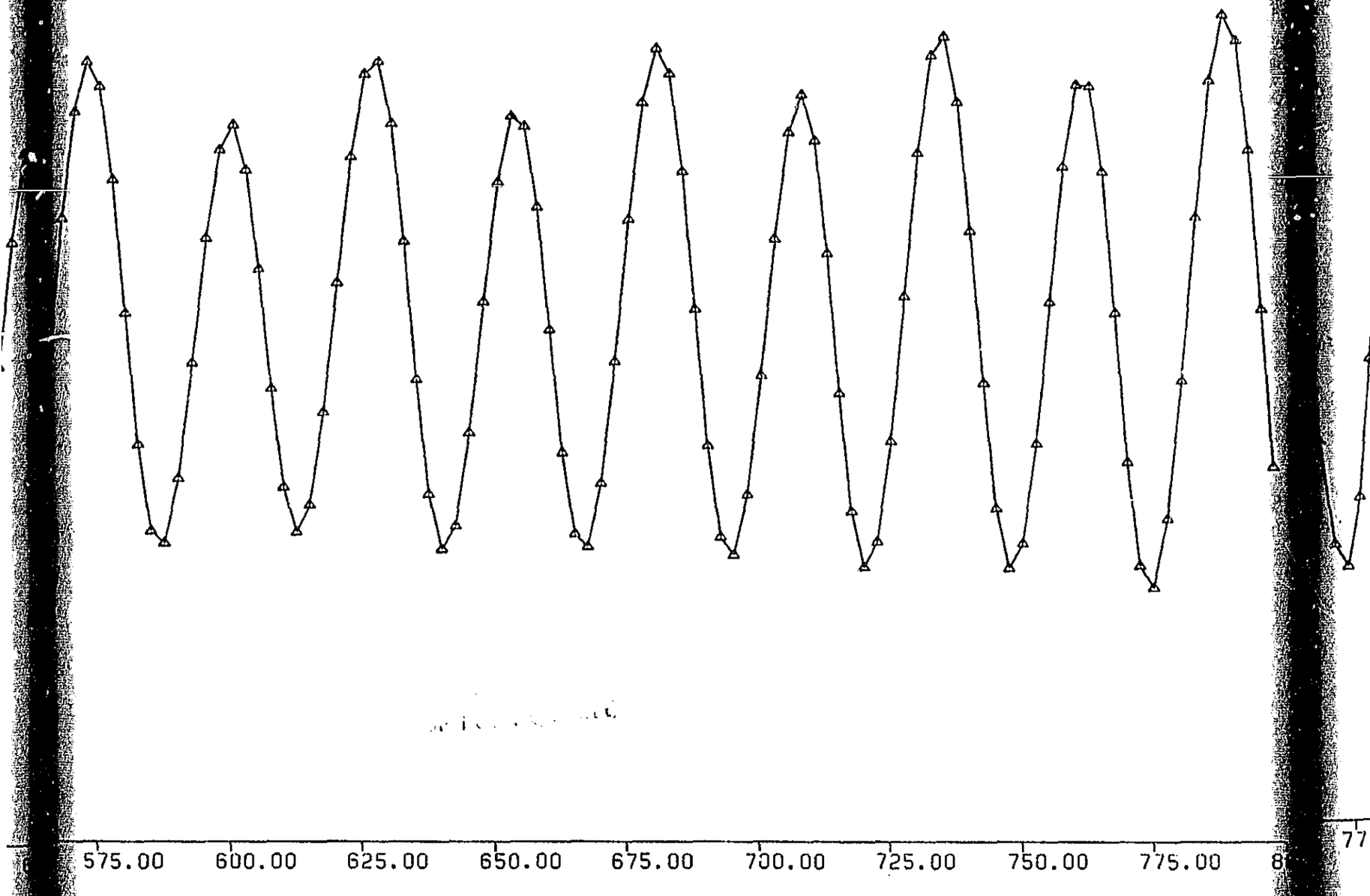

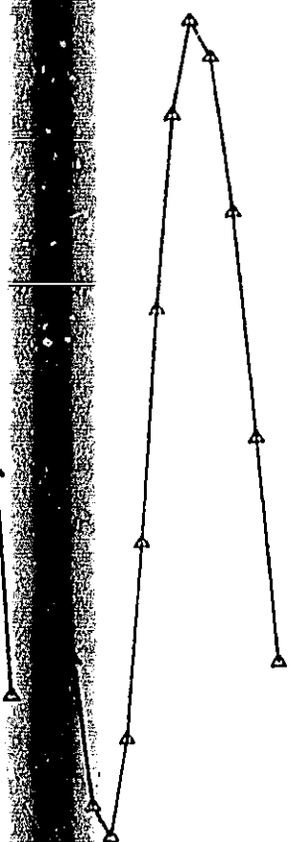

FOLDOUT FRAME

775.00 800.00

Figure B

MASS SYMBOL

2 A

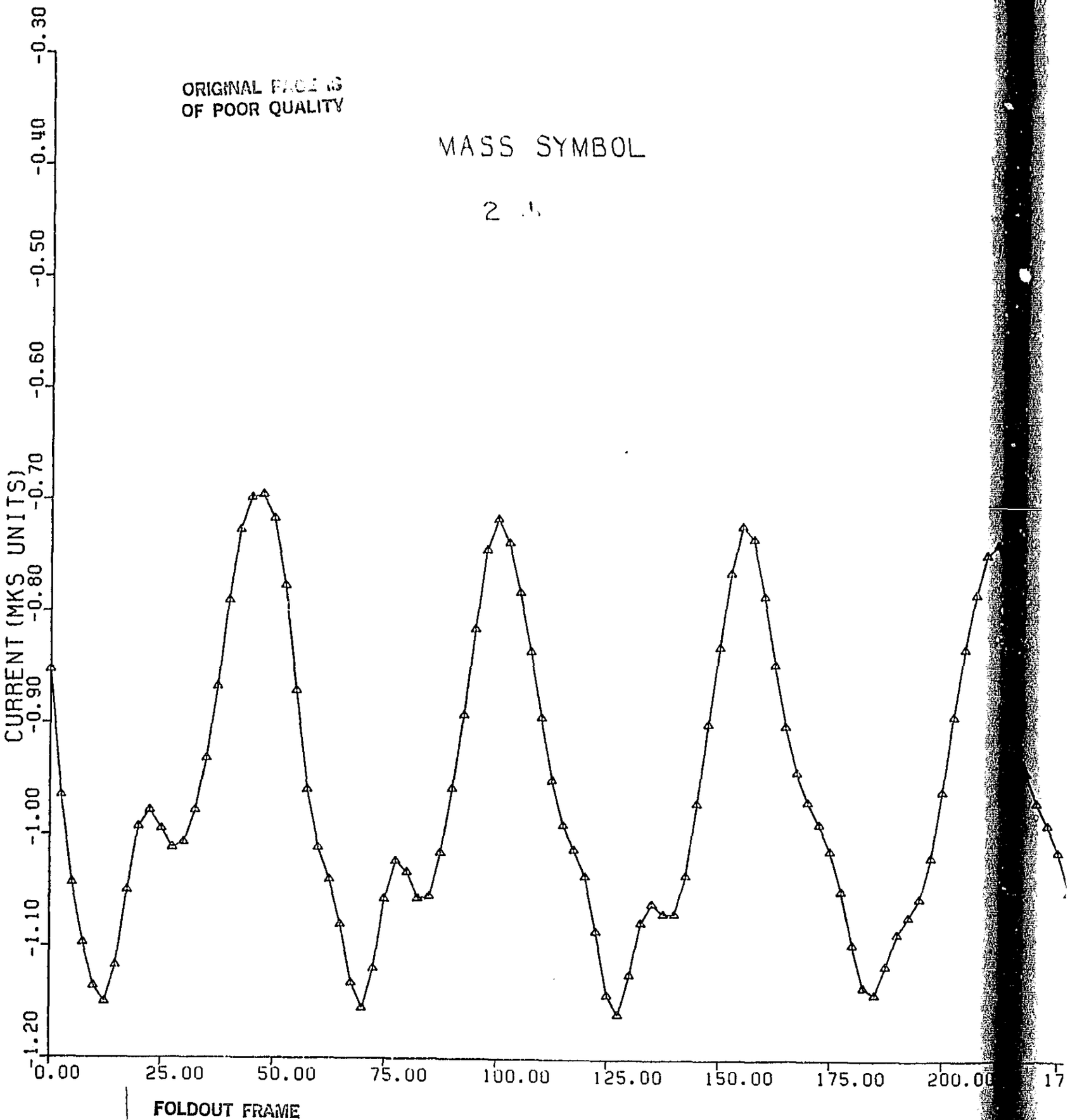

FOLDOUT FRAME

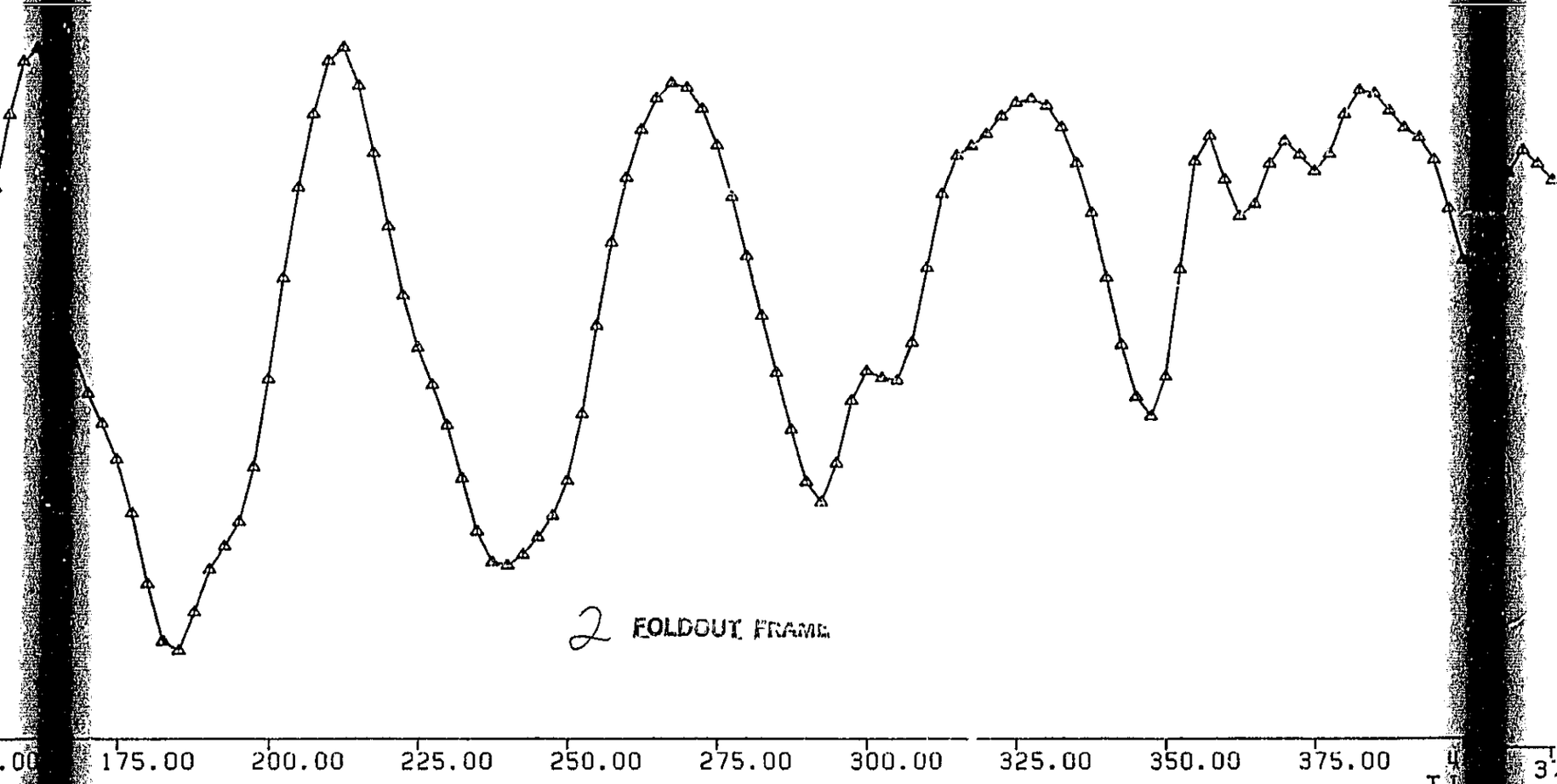

2 FOLDOUT FRAME

3 FOLDOUT FRAME

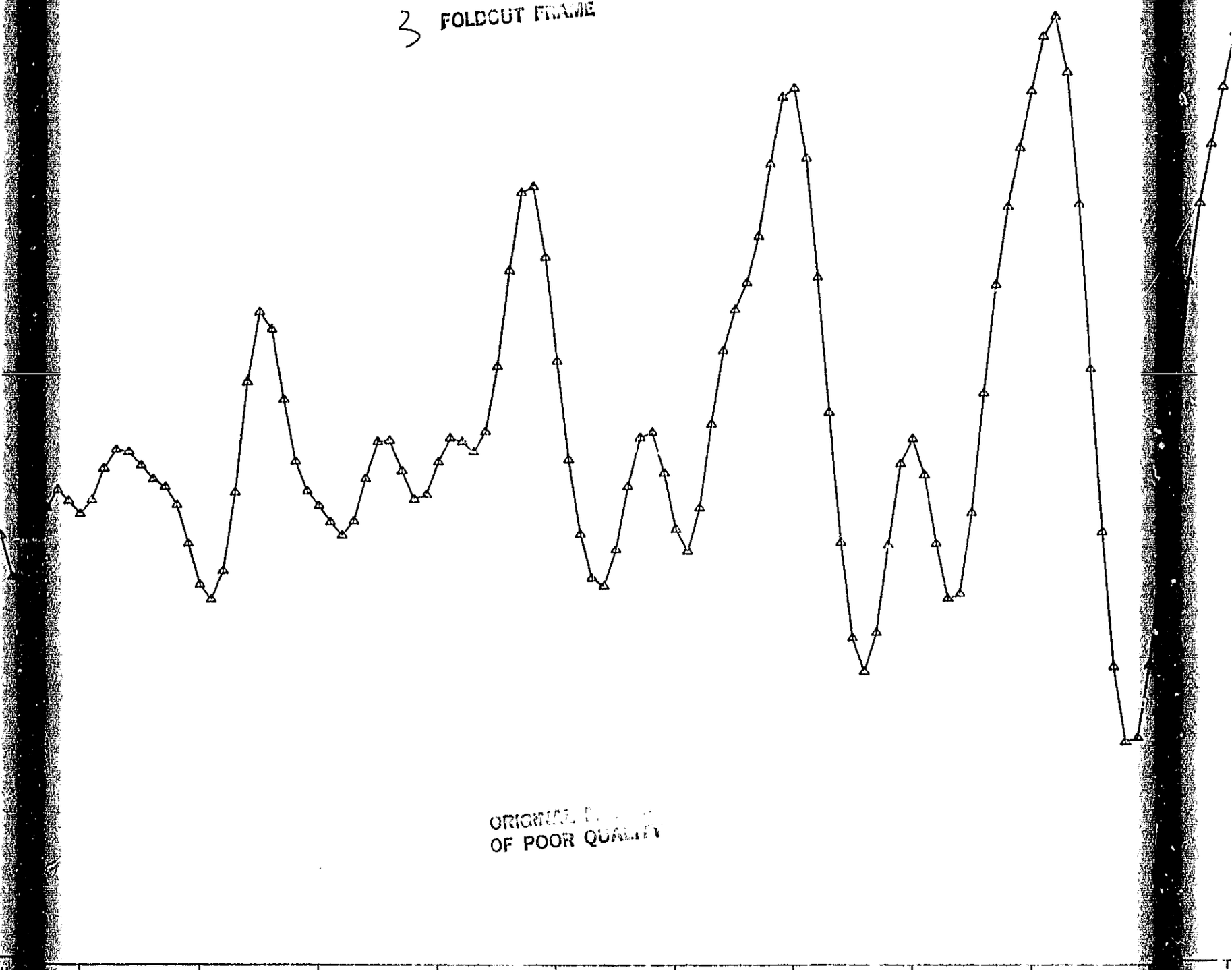

375.00 400.00 425.00 450.00 475.00 500.00 525.00 550.00 575.00

TIME $\times 10^2$

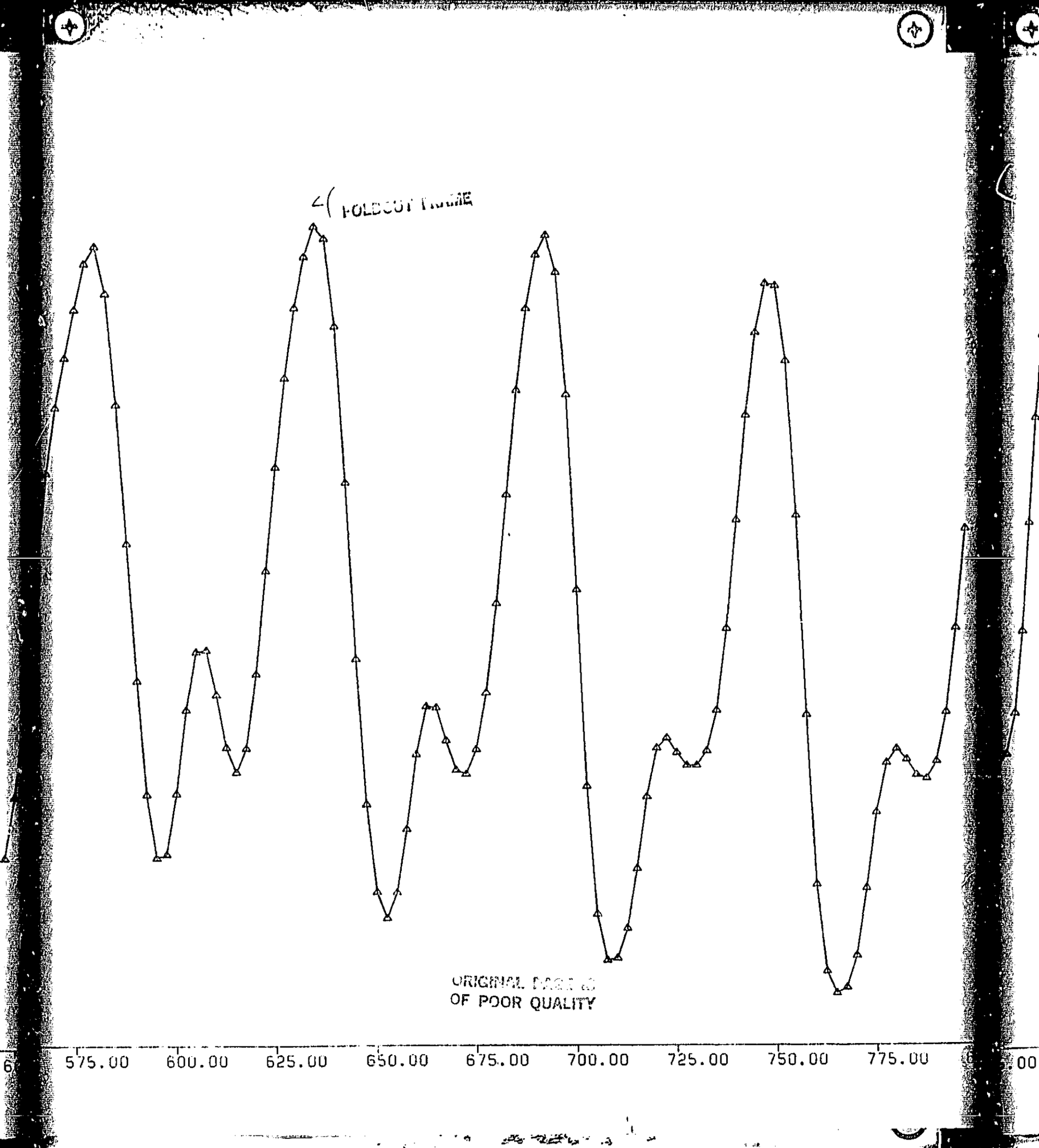

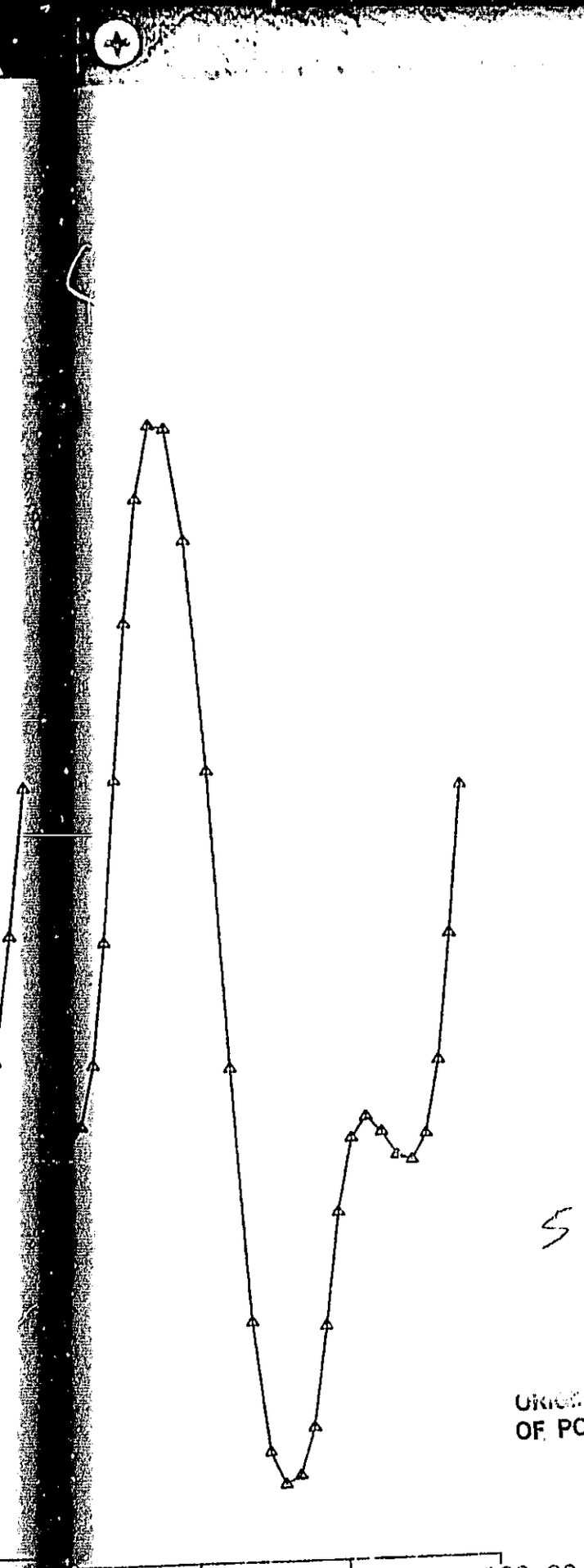

FOLDOUT FRAME

ORIGINAL PAGE IS
OF POOR QUALITY

Figure C

Table 1 below lists the mean value and the r.m.s. deviation of various quantities for the run, along with the rescaled value of the current that actually produces this dynamic response.

Table 1

	Average Value	R.M.S. Value	Minimum Value	Maximum Value
In-Plane Displacement	186 m	242 m	-315 m	+718 m
In-Plane Angle	0.53 deg	0.69 deg	-0.9 deg	2.06 deg
Out-of-Plane Displacement	2.7 m	495 m	-897 m	+930 m
Out-of-Plane Angle	0.01 deg	1.42 deg	-2.57 deg	2.67 deg
Rescaled Current	-1.70 A	.34 A	-.76 A	-2.32 A
$\vec{V} \times \vec{B} \cdot \vec{\ell}$	-3403 v	696 v	-1532 v	-4640 v

Table 1. Summary of the dynamic response during the entire station-keeping phase (electrodynamic mission) of a TSS system without damping.

The out-of-plane oscillation could be theoretically reduced in a couple of different ways. Probably the most efficient would be the use of electrodynamic damping since it is a conducting tether. This technique is discussed in detail in the report "Investigation of Electrodynamic Stabilization and Control of Long Orbiting Tethers," G. Colombo, Interim Report, NASA Contract NAS8-33691, March 1981. The electrodynamic damping can be tuned to the out-of-plane oscillation while ignoring the effect on the in-plane oscillation which is easily handled by reel control techniques (as later shown). The electrodynamic damping can be applied during the retrieval along with a reel control technique.

To investigate the effects of damping by reel control, a similar, long duration simulation was run. The tether tension control law makes the tether respond as a highly visco-elastic medium. For this reason the control law was simulated by assuming an artificial tether stiffness and damping coefficient that give the same longitudinal dynamic response provided by the reeling mechanism.

In order to maximize the out-of-plane damping effectiveness the longitudinal oscillation frequency was fixed at twice the out-of-plane swing frequency (four times the orbital frequency) and the damping coefficient was chosen as low as $\xi = 0.2$. This low value of the damping coefficient is derived from an in-house preliminary study carried out at SAO. The lower the damping coefficient the larger the energy transfer between the pendular libration and the longitudinal oscillation. However a larger tether length variation corresponds to a smaller damping coefficient so that the attainable values are lowerly limited. $\xi = 0.2$ appears to be a good compromise in order to avoid excessive tether lengthening due to the actual libration amplitude during station-keeping. In this simulation the overestimated effect (by a factor of two) of the electrodynamic torque was compensated by halving the current in the tether. The results obtained represent therefore the worst case dynamic response of the system with the tether resistance presently planned by MMA (the actually achievable current in twice as much the one shown in Figure F). In-plane response, out-of-plane response and current are plotted in Figure D, E and F respectively. As expected the values of the oscillation amplitudes are very close to one half those obtained in the other simulation (except the in-plane that is affected by the damping). This means that the dynamic response (at least for small oscillation) is linearly dependent on the

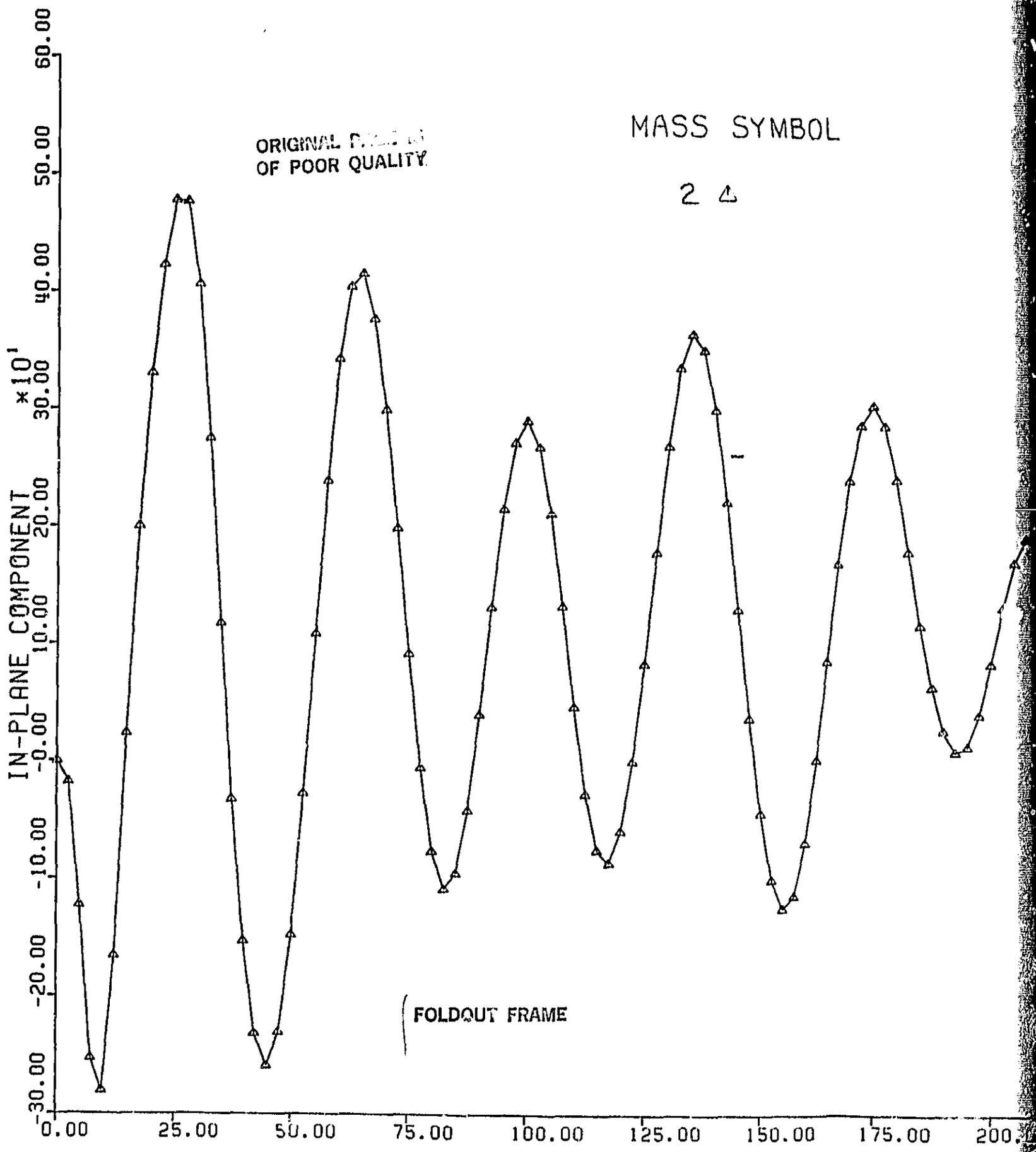

FOLDOUT FRAME

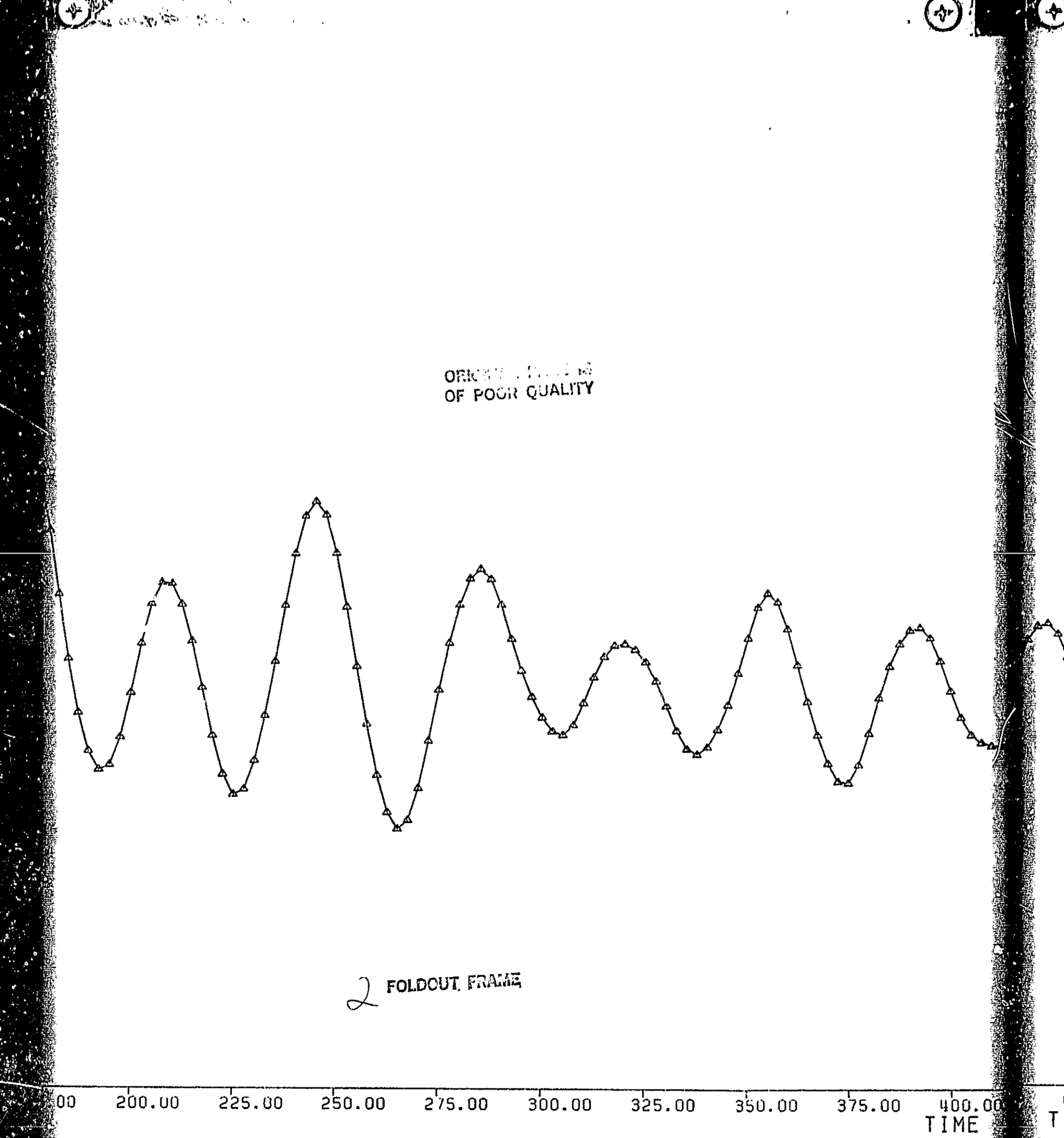

2 FOLDOUT FRAME

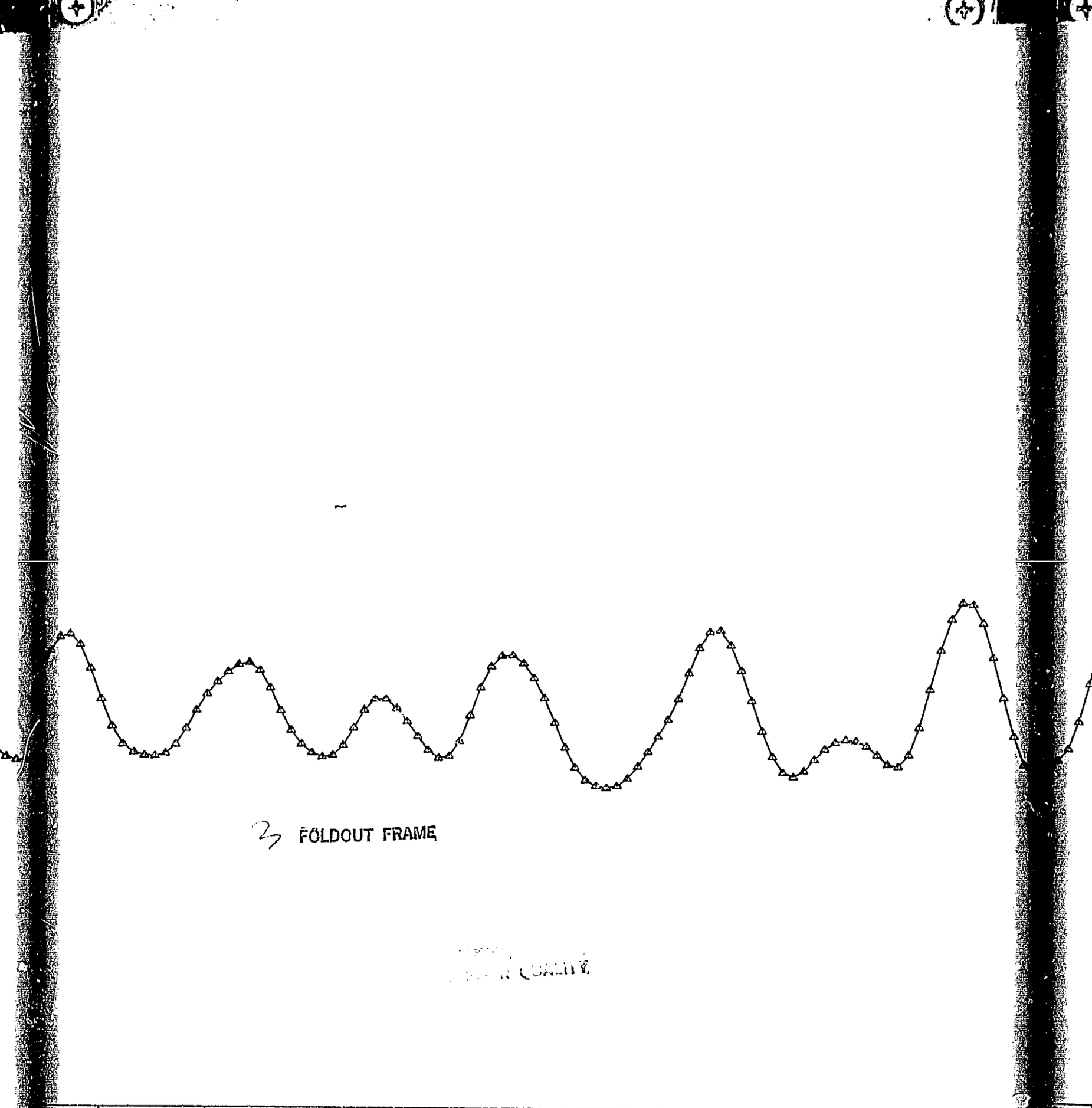

FOLDOUT FRAME

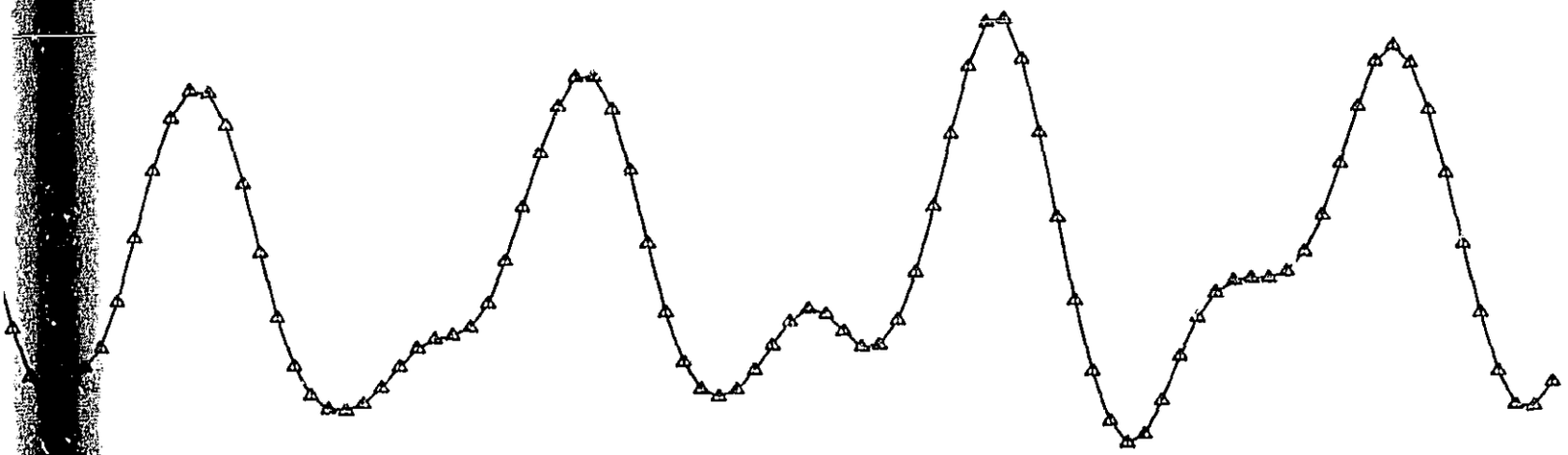

4 FOLDOUT FRAME

Figure D

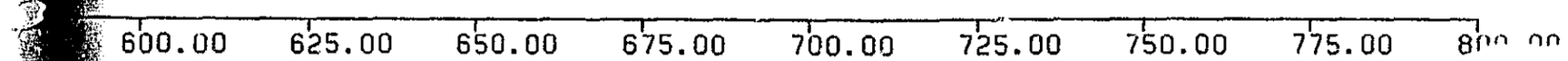

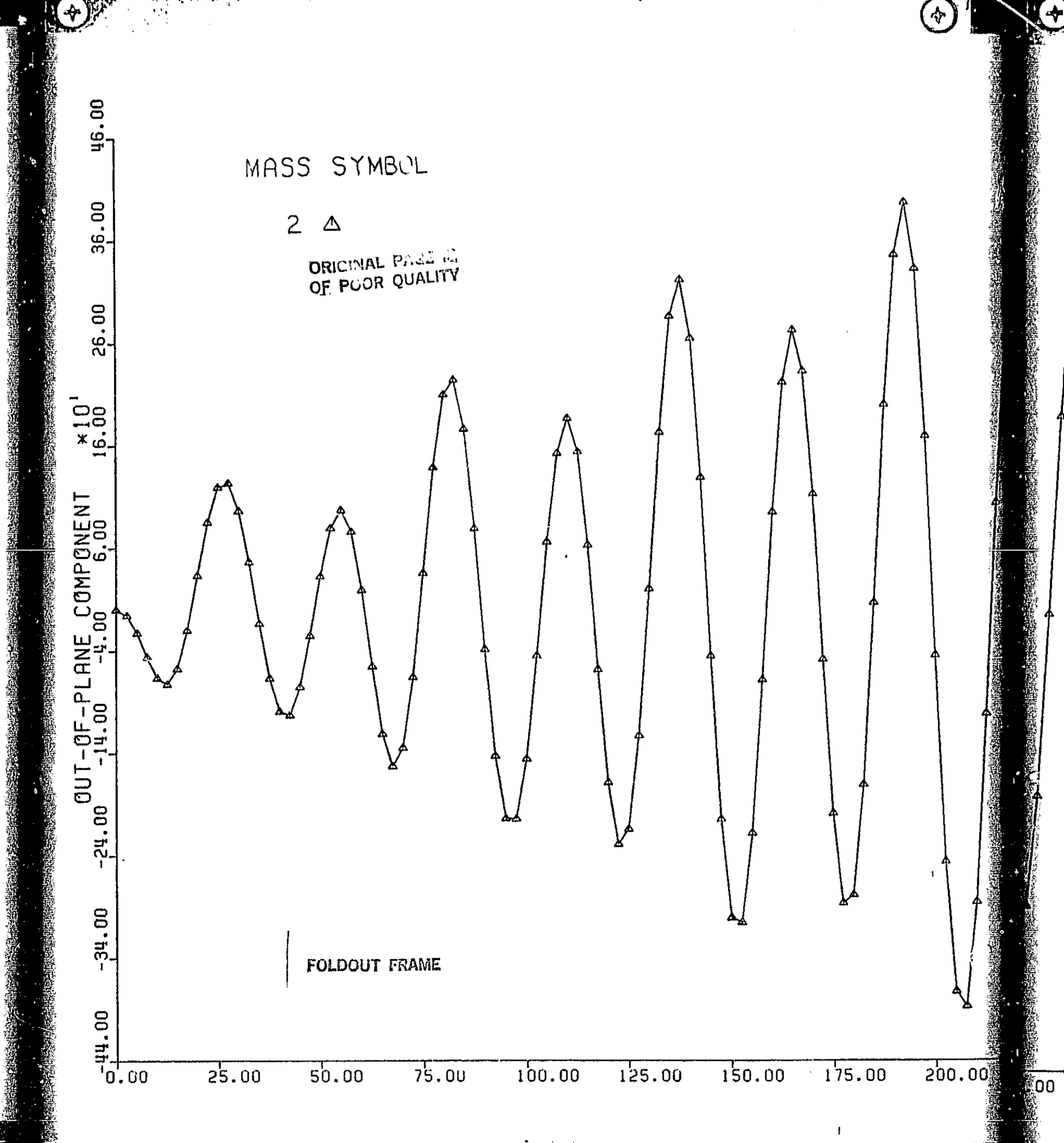
MASS SYMBOL
2 Δ
ORIGINAL PAGE IS
OF POOR QUALITY
OUT-OF-PLANE COMPONENT *10¹
46.00
36.00
26.00
16.00
6.00
-4.00
-14.00
-24.00
-34.00
-44.00
0.00
25.00
50.00
75.00
100.00
125.00
150.00
175.00
200.00
FOLDOUT FRAME

2 FOLDOUT FRAME

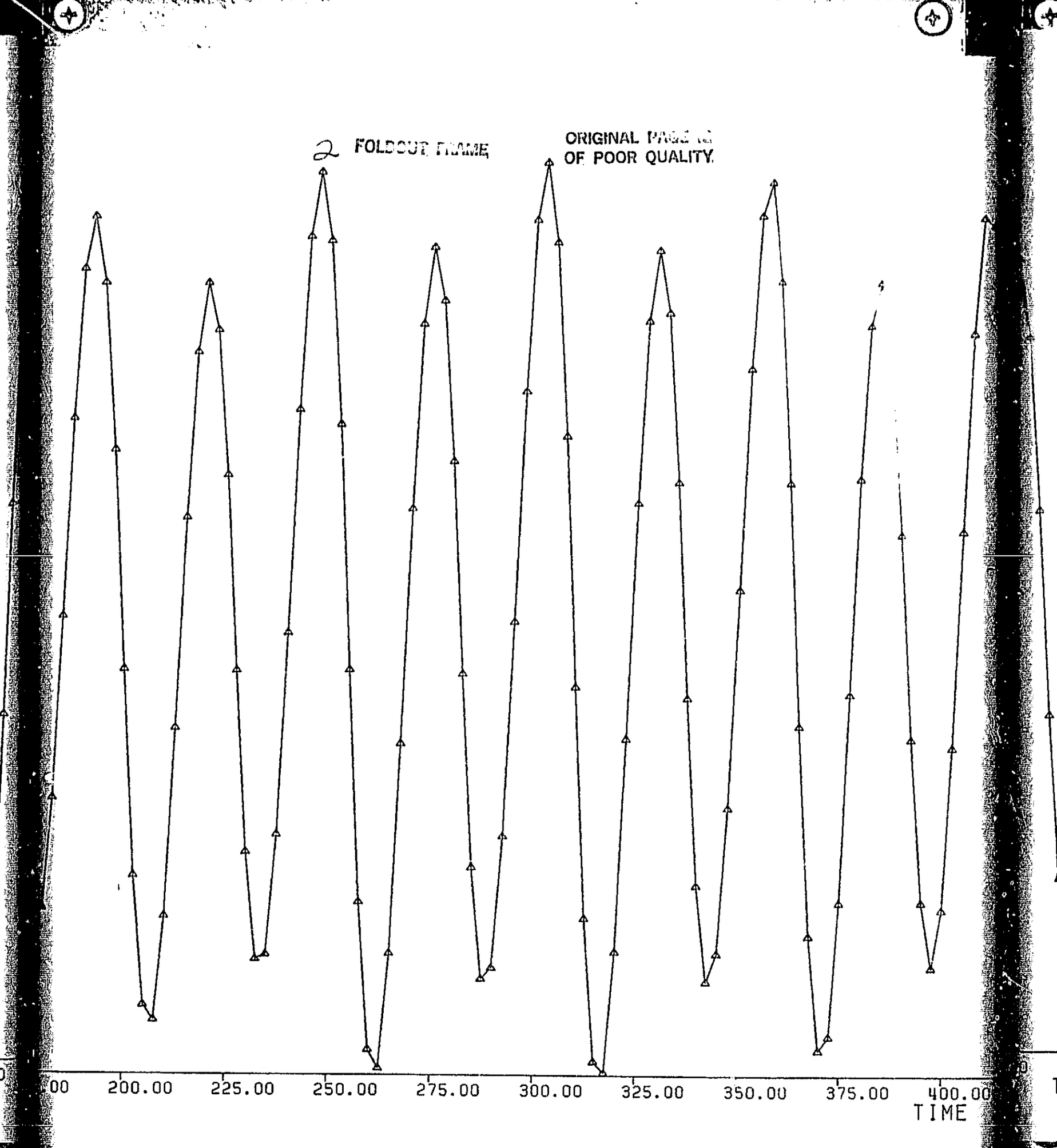

ORIGINAL PAGE IS
OF POOR QUALITY

3 FOLDOUT FRAME

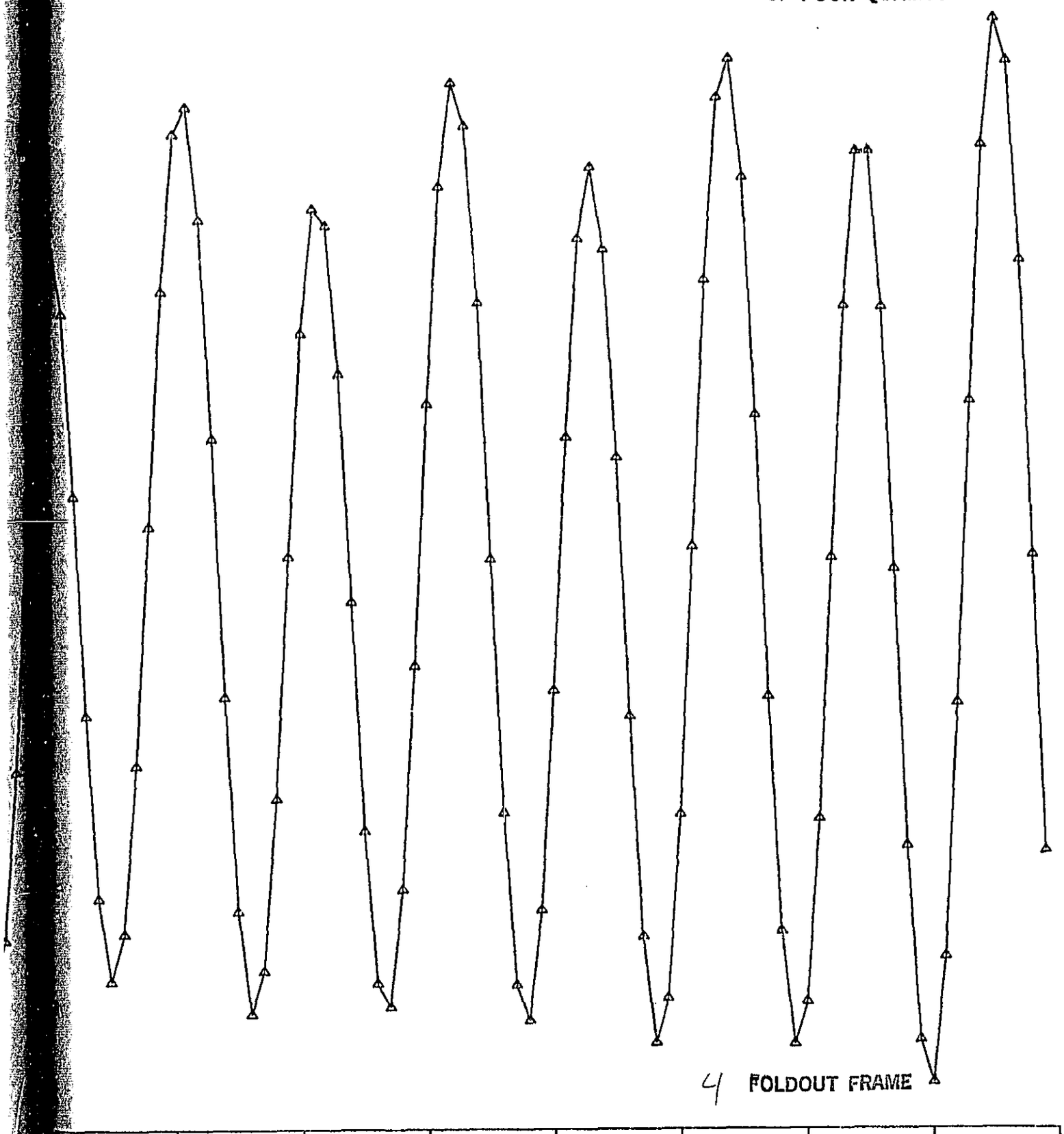

4 FOLDOUT FRAME

Figure E

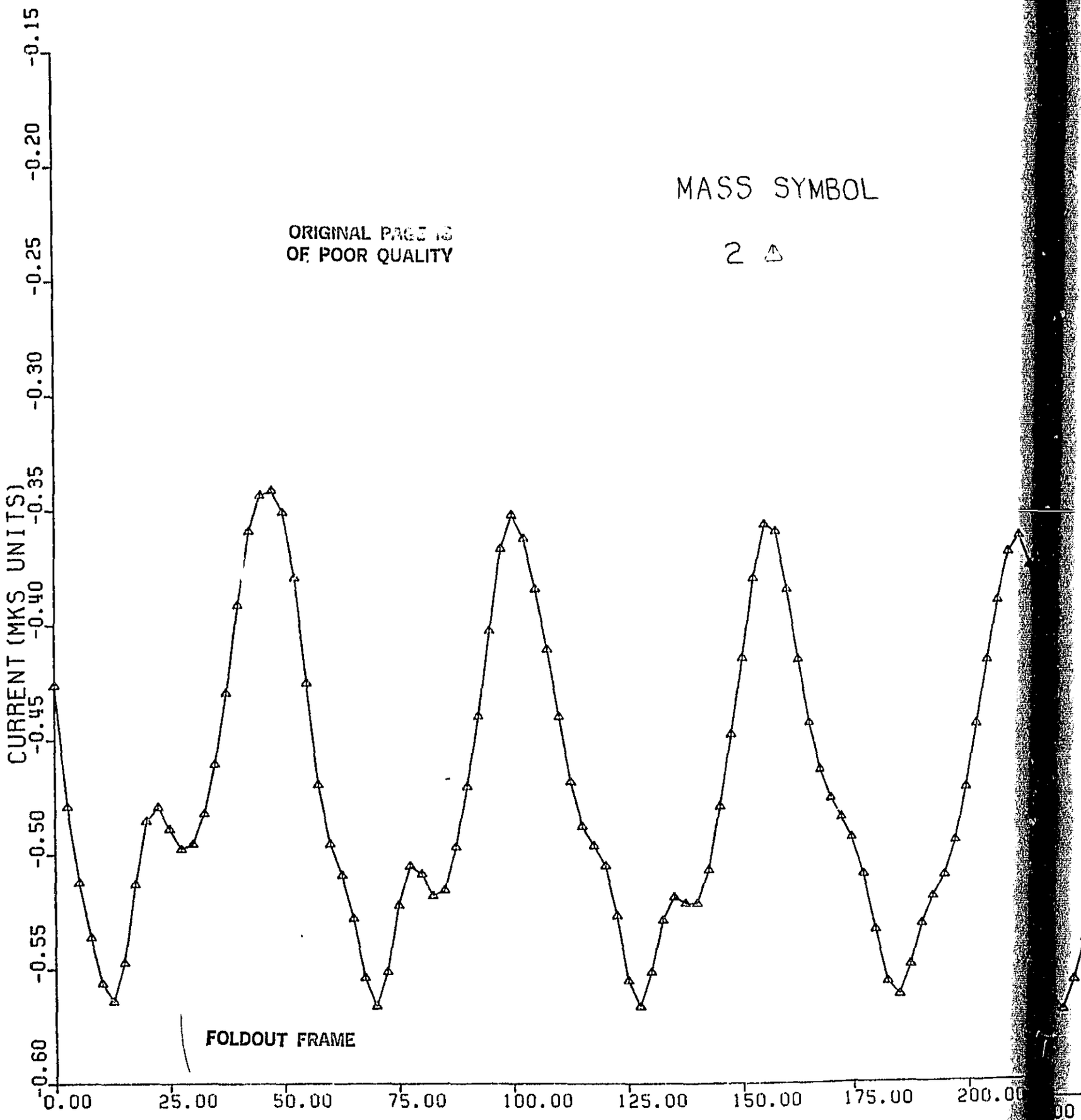
MASS SYMBOL
2 △
ORIGINAL PAGE IS
OF POOR QUALITY
CURRENT (MKS UNITS)
-0.15
-0.20
-0.25
-0.30
-0.35
-0.40
-0.45
-0.50
-0.55
-0.60
0.00
25.00
50.00
75.00
100.00
125.00
150.00
175.00
200.00
FOLDOUT FRAME

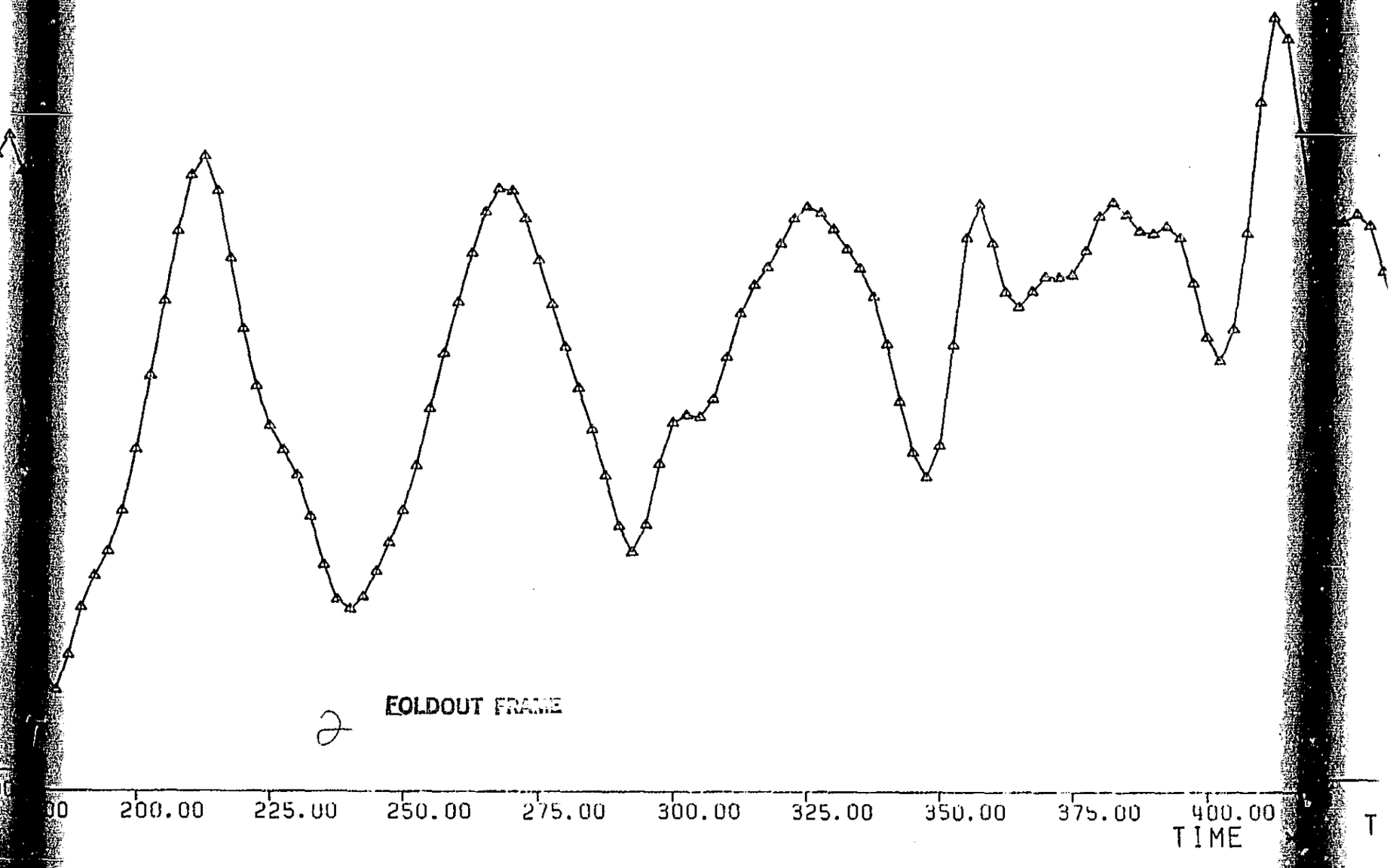

FOLDOUT FRAME 2

ORIGINAL PAGE IS
OF POOR QUALITY

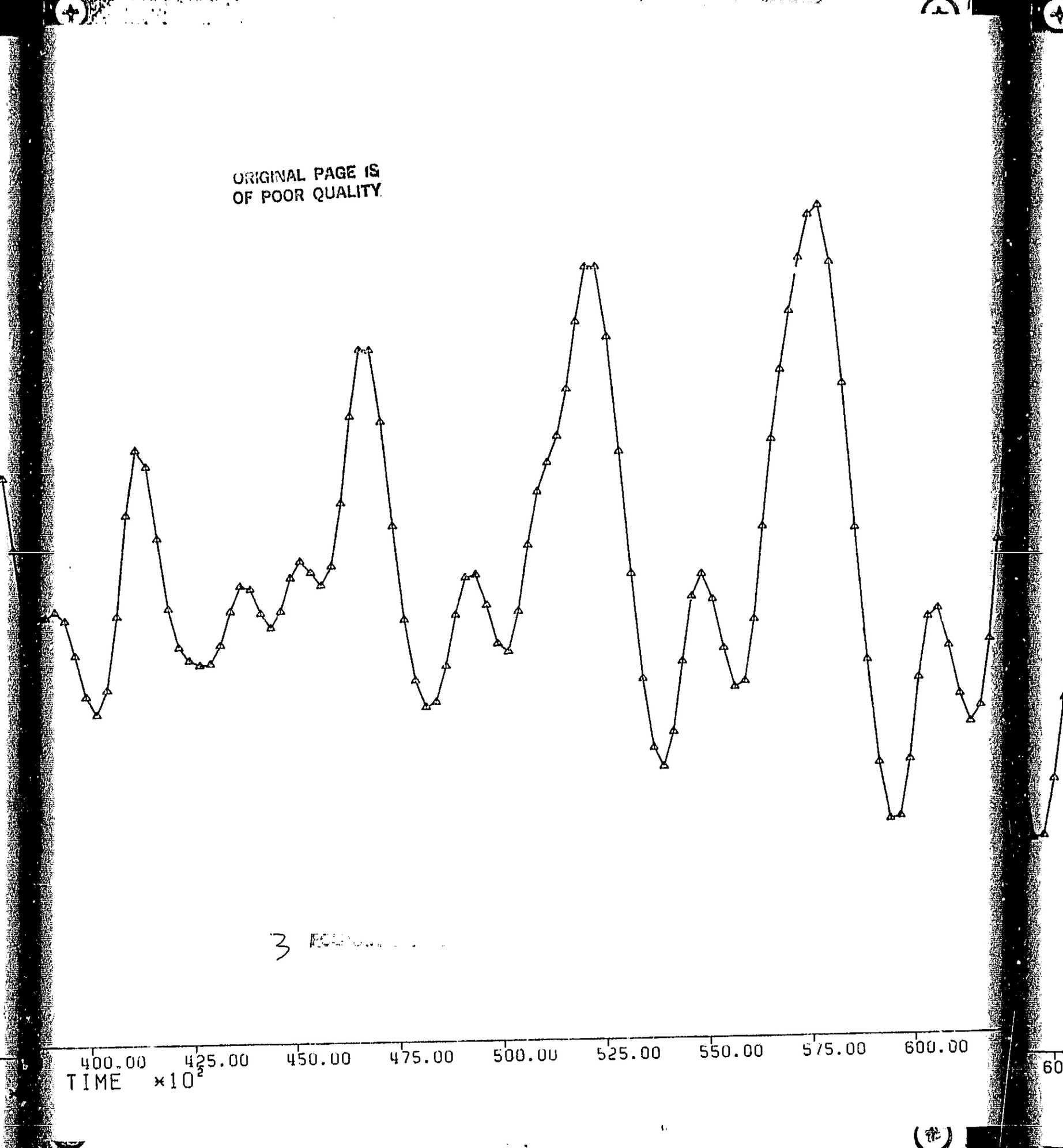

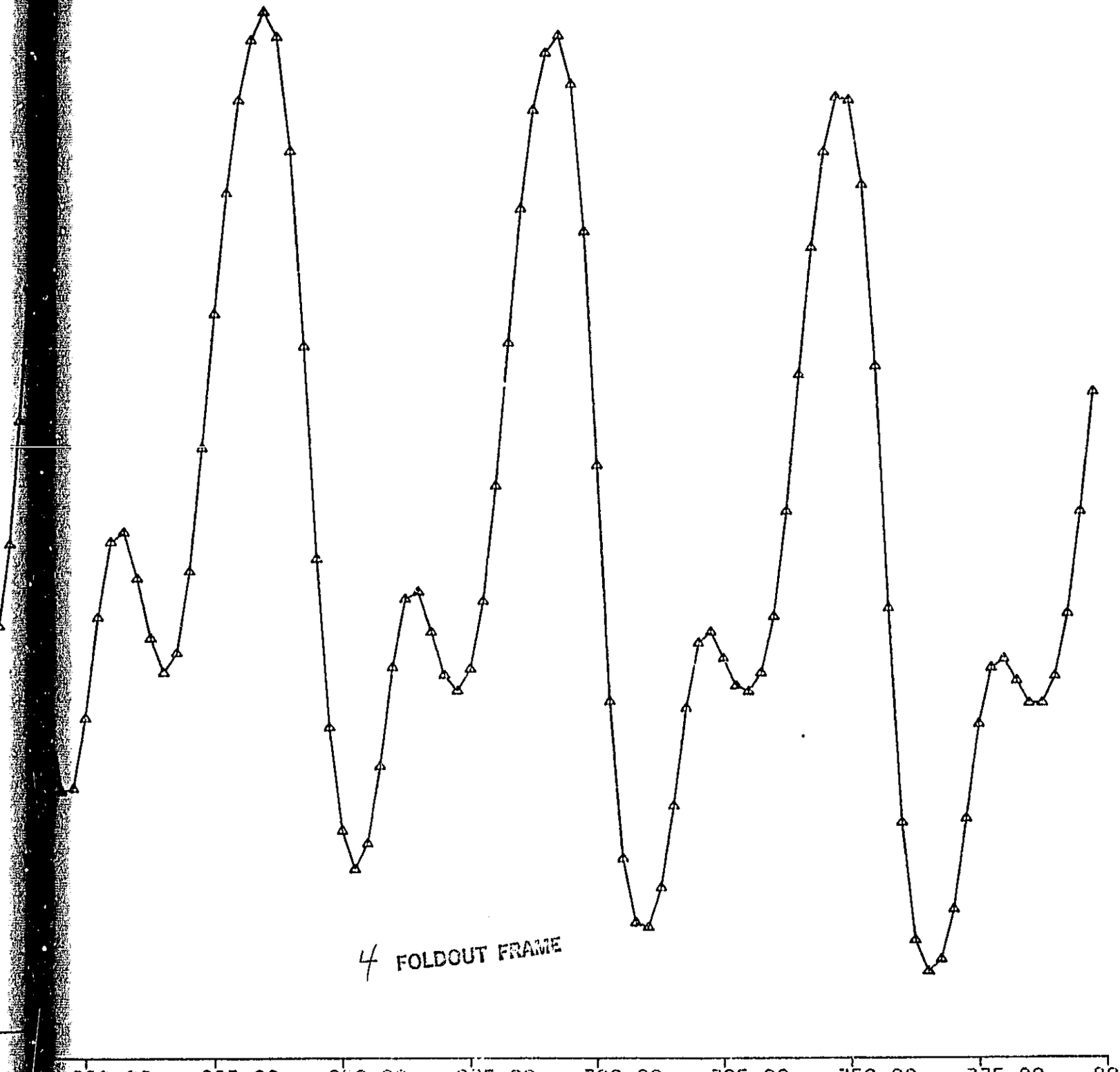

4 FOLDOUT FRAME

Figure F

current; the model adopted for the electrodynamic torque is therefore fully acceptable. Results from the simulation show that the out-of-plane oscillation is almost unappreciably affected by the damping (as suspected). The out-of-plane damping depends, by the way, on the square of the out-of-plane oscillation amplitude and it is therefore very poor for amplitude around one degree. The in-plane, on the contrary, benefits from the damping (even if the tether control is tuned to the out-of-plane) so that the in-plane transient oscillation caused by the current activation (step function) is reduced, after 8 hrs., to its steady state value. A tether control tuned to the in-plane oscillation (as presently done by MMA) is even more effective to damping out the in-plane oscillation. It is therefore more convenient to handle the in-plane libration by tether control and to damp (if deemed necessary) the out-of-plane libration by current control. In Table 2 the most important results of this simulation are summarized. In this table the current is rescaled (multiplied by a factor of 2) to the value that actually produces the dynamic response shown in the upper lines.

Table 2

	Average Value	R.M.S. Value	Minimum Value	Maximum Value
In-Plane Displacement	88 m	110 m	-280 m	477 m
In-Plane Angle	0.25 deg	0.32 deg	-0.8 deg	1.37 deg
Out-of-Plane Displacement	0.9 m	239 m	-433 m	451 m
Out-of-Plane Angle	$2.6°\times10^{-3}$	0.68°	-1.24°	1.29°
Rescaled Current	-0.84 A	0.16 A	-0.38 A	-1.14 A

Table 2. Summary of the dynamic response during the entire station-keeping phase (electrodynamic mission) of a TSS system with positive damping.

Note that the current adopted is the maximum attainable with the present tether resistance and plasma contactors at both tether ends (satellite and Orbiter). The current in the tether is resistively limited and therefore depends on the interaction between the tether and the magnetic field only (no active control). The current is switched on abruptly (step function) and the dynamic response represents, therefore, a worst case condition. Since the out-of-plane dynamics is actually undamped the overshoot of the system after the step function activation is equal to two.

2.1.2 Tether Bowing Due to the Electrodynamic Drag

Measurement of the direction of the subsatellite by observation of the angle of the tether will be subject to error as a result of the curvature of the tether caused by drag and electrodynamic forces. Calculations have been done to estimate the size of the error and provide a possible means of correcting measurements for tether curvature.

A program called CURVES is available at SAO for calculating the equilibrium shape of a tether under the influence of electrodynamic and gravity gradient forces. The program uses the numerical integrator from SKYHOOK to generate the shape of the curve given the position, orientation and tension of the wire at some point.

Neglecting the effects of atmospheric drag, the tether must be vertical at the point of attachment at the subsatellite. The tension must be equal to the gravity gradient force on the subsatellite. Assuming that the curvature of the tether is small, the altitude of the subsatellite must be that of the Shuttle plus the length of the tether.

Program CURVES has been run for the case of a 550 kg subsatellite at the end of a 20 km tether deployed upward from the Shuttle at an altitude of 296 km. The resistance of the tether is .2 ohms/meter (4000 ohms total), and the current is resistively limited. If the magnetic field (B) is $.3 \times 10^{-4}$ w/m^2, and the orbital velocity is 7,730 km/sec, the induced voltage is about 4600 volts so that the current is 1.15 amps. For an orbital angular velocity of .001158 radians per sec the gravity gradient force on the subsatellite is 45.8 newtons. The electrodynamic force $I\ell B$ is .69 newtons. The density of the wire is 8.35 kg/km. This information is needed to integrate the tension which affects the curvature. The integration was started at x = 0, and y = 20,000 meters, where x is measured along track and y is along the local vertical. The generated curve intersected the x-axis 133.84 meters from the origin with a tension of 52.75 newtons and an angle of .013080 radians (.7494 degrees). The line of sight angle to the subsatellite is .006692 radians (.3834 degrees), so that the error by measuring the tether angle for tracking the subsatellite is .3660 degrees (see Figure G-a). At the upper end the deviation from the line of sight is of course .3834 degrees since the integration was started with the wire vertical at the subsatellite end. The radius of curvature of the wire at the upper end is 1,327,000 meters and at the Shuttle end is 1,529,000 meters.

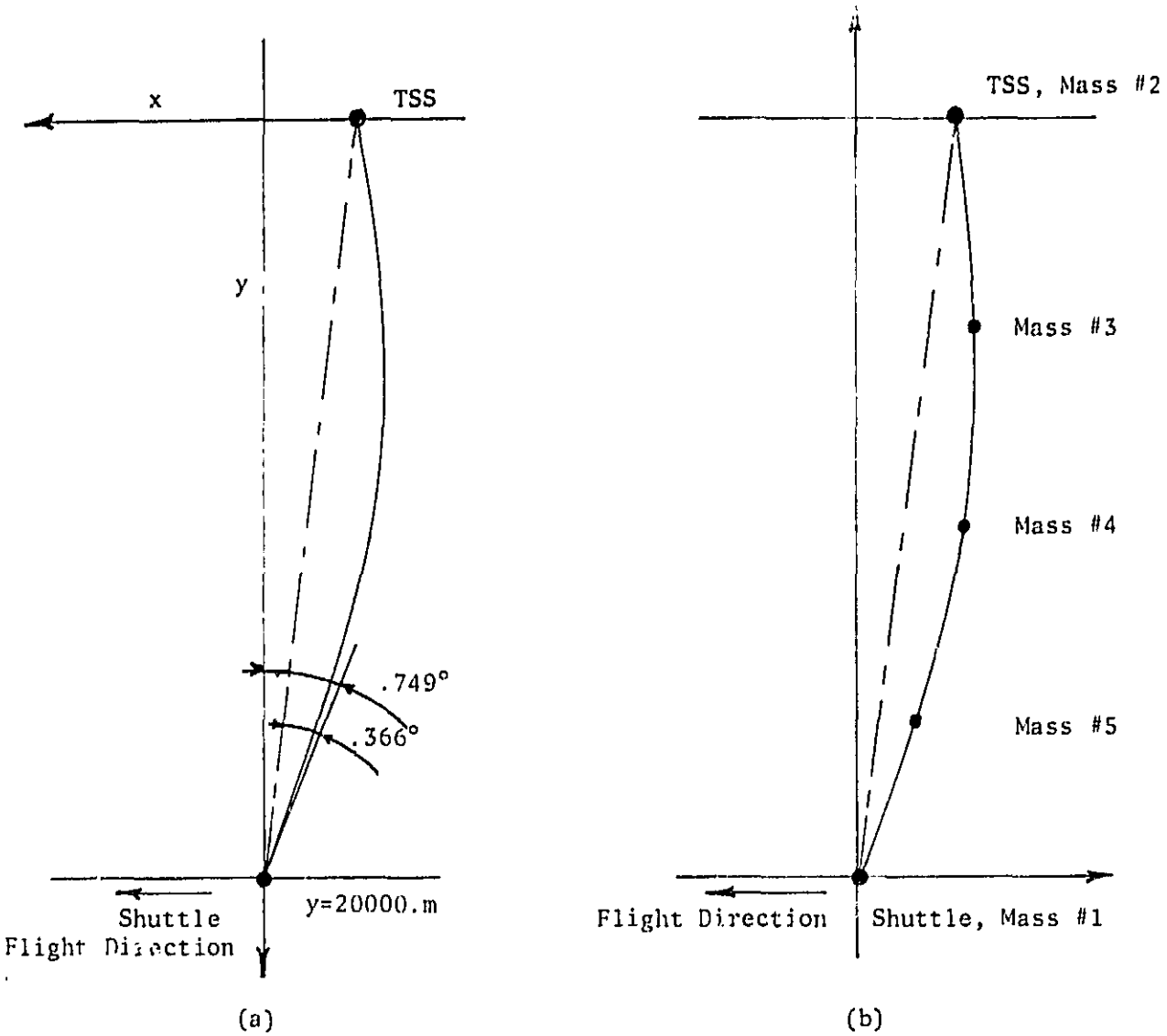

Figure G - Geometry for the Tether Bowing Analysis (Figure not to Scale)

(a) - Reference frame and deflection angles as computed by the CURVES computer code

(b) - Reference frame and mass discretization as in the SKYHOOK computer code.

The deviation of the tether angle from the line of sight can be calculated approximately from the curvature of the wire. The curvature is related to the tension and the electrodynamic force per unit length by the equation $dT/ds = T/R_0$. The force per unit length is $IB = 3.45 \times 10^{-5}$ newtons/meter. The gravity gradient force on the wire is 6.95 newtons and that on the subsatellite is 45.8 newtons so that the tension at the Shuttle end is 52.75 newtons. The values of 45.8 and 52.75 newtons give curvatures of 1,327,000 and 1,529,000 meters as calculated in the integration program. A radius of curvature of 1,529,000 meters gives a change in angle of .75 degrees over 20,000 meters. The deviation from the line of sight would be half this or .375 degrees. This is in reasonable agreement with the deviation from line of sight calculated by the integration program.

A simulation has been run with the SKYHOOK program using 5 mass points (three representing the wire) to further study the deviation from line of sight with a current carrying tether (see Figure G-b). The simulation uses a 2.59 mm tether with each mass point having a mass of 41.75 kg. The Shuttle mass is 101.3379 metric tons and the subsatellite is 550 kg. The magnetic pole is oriented 90° west of the starting point of the orbit. The tether is initially vertical and is deflected to the rear, oscillating about the equilibrium angle. The program produces a file of in-plane and out-of-plane components for each mass point. The pendular part of these displacements has been removed in order to study the deflection of the wire directly. Figure H and I show the deflection of each mass point vs. time. The wire current is also plotted in Figure J. Mass 1 is the Shuttle, mass 2 is the subsatellite, mass 3 is next to the subsatellite, mass 4 is in the middle of the wire, and mass 5 is next to the Shuttle. The amplitude of the in-plane oscillation of masses 3 and 5, soon after the current

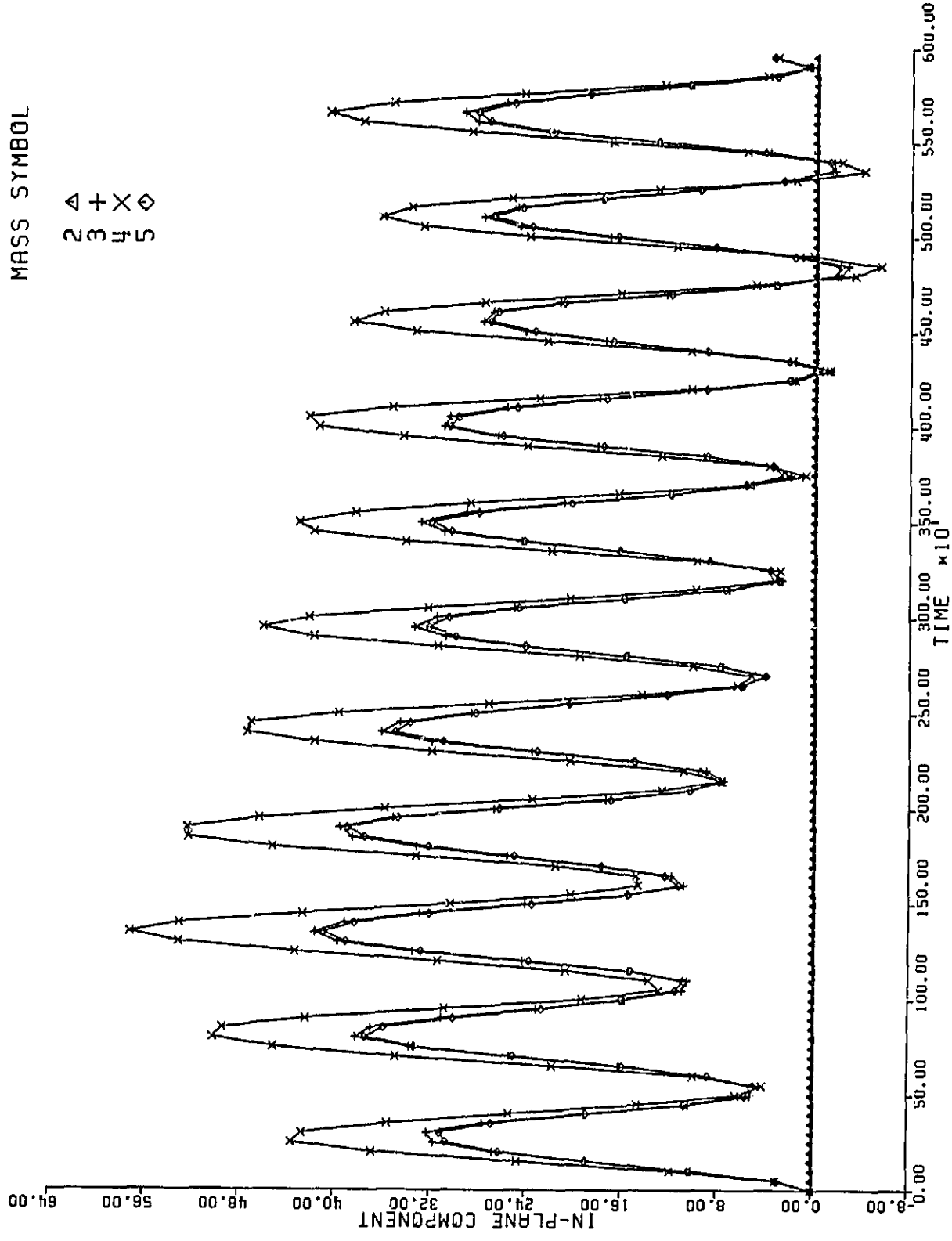

Figure H - Tether deflection wrt. the Orbiter/Satellite line of sight.
Pendular libration removed (MKS Units).

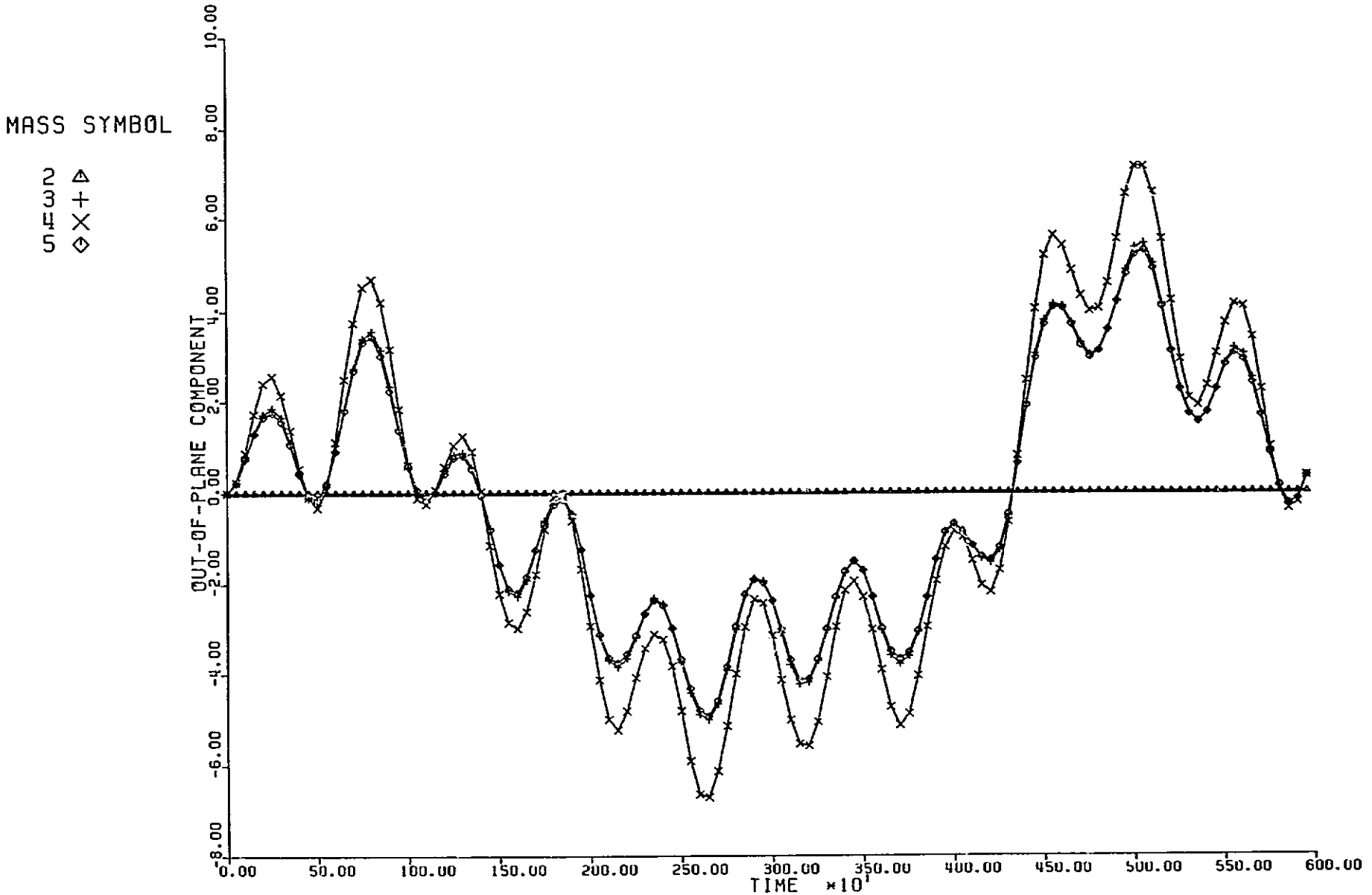

Figure I - Tether deflection wrt. the Orbiter/Satellite line of sight. Pendular libration removed (MKS Units).

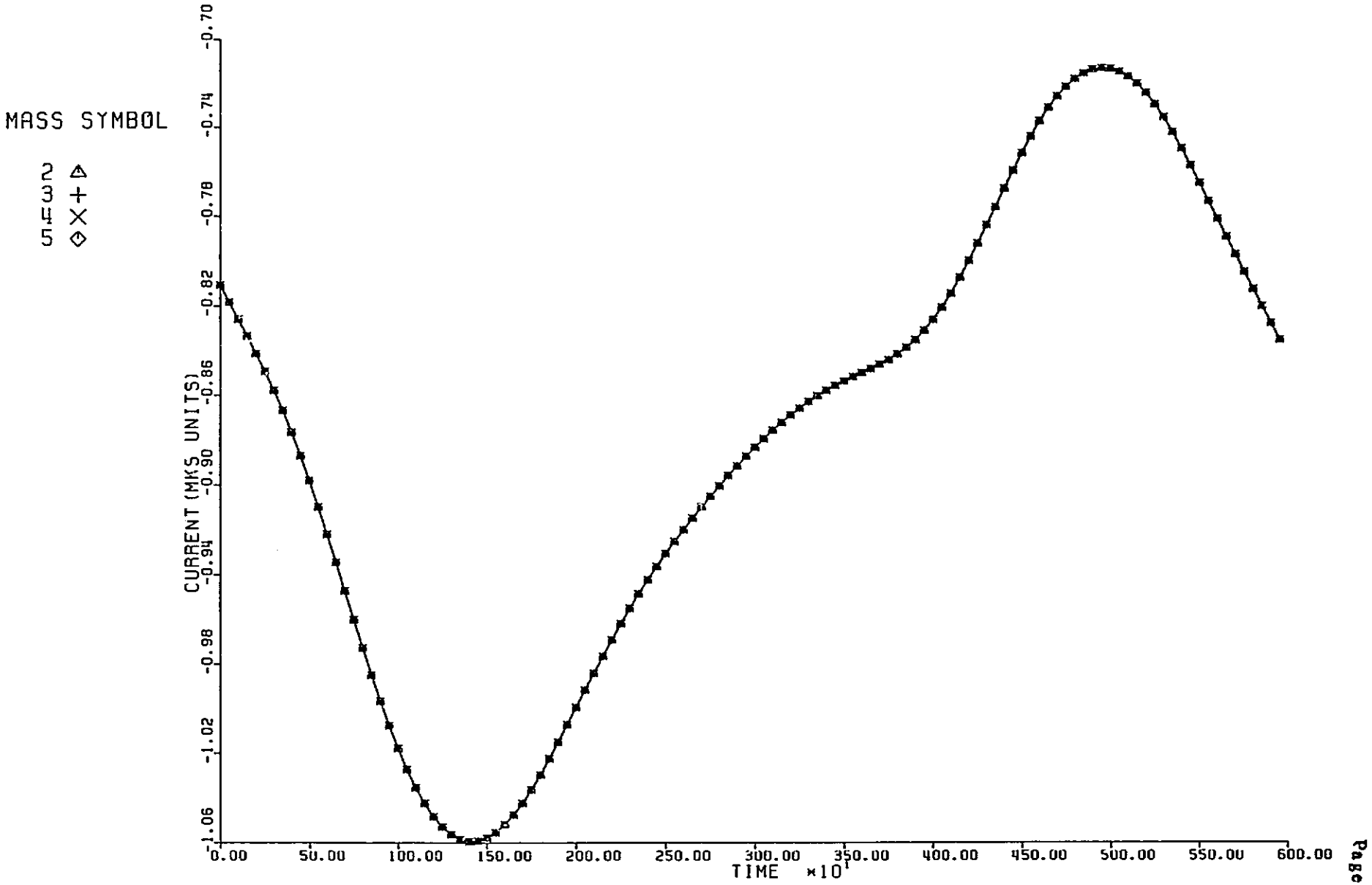

Figure J - Current in the tether vs. time, used to compute the tether deflection. Tether resistance is 4kΩ . Plasma contactors at both tether ends.

activation, is about 30 meters and for mass 4 it is about 44 meters. Since each segment of wire is 5 km long, the deflection angle at the ends of the wire is about .34 degrees. In order to compare this to the output of program CURVES it is necessary to correct for various differences. In CURVES the current was 1.15 amps and the magnetic field was $.3 \times 10^4$ w/m^2. In the SKYHOOK run the initial current is .81 amps and the z-component of the magnetic field is $.256 \times 10^{-4}$ w/m^2. Since the wire is oscillating about the equilibrium displacement in the SKYHOOK run, the amplitude should be twice as great as the amplitude of the equilibrium displacement. Because of discretization the angle computed from the wire mass adjacent to the end gives the mean angle about 3/4 of the way from the center of the wire rather than the angle at the end of the wire. Assuming the curvature is nearly constant, the angle is too small by a factor of about 3/4. Taking the deflection of .38 degrees from program curves and applying all the correction factors, 2 x (3/4) x (.81/1.15) x (.256/.3), gives .34 in agreement with the results from SKYHOOK. In program CURVES the maximum deflection at the center (with the pendular part removed) is about 32.5 meters. To compare this with SKYHOOK the amplitude must be multiplied by the factors 2 x (.81/1.15) x (.256/.3) = 1.2. Multiplying 32.5 x 1.2 = 39 meters which compares fairly well with 44 meters from SKYHOOK. The amplitude of the oscillations in the out-of-plane direction is about 2 or 3 meters. The y-component of the magnetic field is $.021 \times 10^{-4}$ w/m^2 which is 8% of the z-component. Multiplying 30 meters by .08 gives 2.45 meters which agrees with the observed amplitude of the out-of-plane oscillation. In addition to the oscillations, the in-plane and out-of-plane displacement show shifts in the mean value through the orbit as the magnitude of the $\vec{I} \times \vec{B}$ force slowly changes. The period of the transverse oscillations is about 535 seconds both in-plane and out-of-plane. The period of the fundamental

fundamental transverse mode is $2\ell/v$ where the velocity of propagation v is $\sqrt{T/\rho}$. Taking T = 46 newtons, $\rho = 8.35 \times 10^{-3}$ kg/m, and ℓ = 20 km gives a period of 539 seconds in agreement with the observed period.

2.1.3 Concluding Remarks

The satellite and tether dynamics during the entire station-keeping phase of the first electrodynamic mission does not appear to be worrisome. The out-of-plane satellite libration builds up to a maximum value of 1.3 deg in a worst condition case: current switched on abruptly, plasma contactors at both tether ends, tether resistance of 4000 ohm (as presently planned by MMA), and no other resistive load in the loop. The build-up is due to a small resonant component (frequency = 2Ω) of the electrodynamic force. The system is however forced out-of-resonance by (most probably) the magnetic pole rotation. Damping out the out-of-plane swing amplitude by tether tension control came out to be uneffective. Current control (if deemed necessary) could be a valid option.

The tether bowing is fairly limited. A conservative value is obtained by multiplying by the dynamic overshoot (a factor of 2) the result obtained with the program CURVES. The maximum deflection (in the middle of the tether) from the line of sight is, therefore, around 65 m. This value is consistent with a maximum angle (at the boom tip) between the tether and the line of sight of 0.767 degrees.

2.2 High Resolution Slack Tether Studies: SLACK2 Model*

2.2.1 Introductory Remarks

Under previous contract, SAO has developed a high-resolution, two dimensional model of a zero-tension tether (Gullahorn, 1983; Colombo, Arnold, Gullahorn and Taylor, 1984).

This model, implemented in the computer program SLACK2, is intended to be similar to SKYHOOK insofar as feasible. As with SKYHOOK, the continuous tether is modelled with the simple "lumped mass" or "ball and spring" approach. A new physical system is constructed by dividing the tether into several segments; each segment is replaced by an equivalent mass at one end and a massless spring connecting this mass to the adjacent segment's mass. The spring generates no force when not stretched; the segment area (for air drag) is mapped onto the end mass. SKYHOOK then applies realistic forces, both internal and external, to each mass and numerically integrates their motions in earth-centered coordinates. SLACK2 operates in a coordinate frame relative to the (infinite mass) Shuttle and applies an idealized set of forces: linearized gravity gradient and Coriolis accelerations; drag; perfectly inextensible (infinite elasticity) connecting segments. This latter idealization means that the segments are "almost always" slack and that when two masses separate to bring a segment into tension they undergo an infinitesimally short "bounce" reversing their motions along the segment direction in their center of mass frame. Both the bounces and the motion of the masses between bounces are analytically soluble, allowing a major increase in efficiency over SKYHOOK, which must numerically integrate difficult differential equations. The motion is restricted to the orbital plane in SLACK2, but this is not a fundamental requirement and a three dimensional version is in preparation.

---

*Contributed by Dr. Gordon E. Gullahorn, SAO

In contrast to these restrictions for improved speed, SLACK2 extends SKYHOOK's capabilities in other directions: initial conditions are generated internally, and non-uniform segment lengths are supported; many more segments are feasible, up to fifty; a vibrating boom is included as the tether attachment point. For more details on the model, see Colombo et al. (1984).

In the current reporting period, SAO has improved and studied SLACK2 and utilized the program in tether break studies:

-- The post-processing plotter was re-created for operation with a changed computer operation system. A printer plotter/lister was created to allow detailed examination of particular variables.

-- Improvements in the coding and some of the numerical routines were made which reduce the run time by a factor of two.

-- A detailed comparison was made between SKYHOOK and SLACK2 results for a particular case. All discrepancies are understood.

-- A protocol for running cases with long tether remnants was developed. Previously, such cases had caused program failure.

-- The effects of tether longitudinal damping were studied.

-- Modifications toward a three dimensional version are underway; initial coding of a simple version is complete.

-- A stability analysis of a very simple version (linear, no Coriolis or drag forces) was initiated.

Several of these topics are discussed in further detail in the sections below.

2.2.2 Comparison of SKYHOOK and SLACK2 results.

SKYHOOK has been exercised, debugged and refined for many years. Since the physical model in SLACK2 is similar to that in SKYHOOK, an obvious way to enhance confidence in SLACK2 is to compare its results with those of SKYHOOK. For a variety of reasons, making this comparison is not as trivial as one might at first expect:

-- SLACK2 incorporates an oscillating twenty meter boom; this is not in SKYHOOK.

-- The initial conditions for SKYHOOK are tedious to compute (by hand) unless one wants to start from an equilibrium configuration with equally spaced masses.

-- SKYHOOK assumes a tether with finite elasticity; SLACK2, infinite. Thus, the instantaneous "bounces" in SLACK2 become brief time periods in SKYHOOK during which the motion is integrated with a stretched tether. These intervals become briefer, and the agreement with SLACK2 better, as the elasticity in SKYHOOK is increased, but there is a limit beyond which SKYHOOK experiences difficulty.

-- SLACK2 assumes a constant density, and this constant is built into the program (for ease of operation). SKYHOOK computes the density as a function of altitude and solar direction.

-- SKYHOOK computes the mass and area/mass, rather than accepting these as input, for each tether segment ... except the terminating one. This exception is undocumented and not clear from the code. The values for the terminating segment must be input as the "subsatellite." (If we were operating with an actual subsatellite instead of a cut tether, the subsatellite mass and area/mass would have to change with the number of tether segments to be correct.)

-- SKYHOOK and SLACK2 use somewhat different drag models: in SLACK2 area of each segment never varies; in SKYHOOK, the area perpendicular to the direction of motion is used. SLACK2 uses the total segment area, multiplied by a fudge factor of 0.75 to approximate the projection effect. The SLACK2 model was chosen primarily for computational reasons, but it is not a priori obvious that the SKYHOOK projected area model is more appropriate for a slack, possibly crumpled, tether segment.

-- SKYHOOK and SLACK2 use different conventions for the sign of the "in-plane" coordinate in the plot file: in SLACK2 the "in-plane" axis points in the direction of orbital motion (a positive value indicating further "along orbit" than the reference Shuttle), while SKYHOOK chooses the axis pointing back along the orbit (this was found by experiment, and was apparently done to make the successive configuration plots more consistent since the Shuttle moves from left to right in the successive plots and with the normal conventions the positive in-plane direction would be to the left).

Keeping these considerations in mind, the comparison runs were made (after several iterations) as follows:

Step 1: SLACK2 was run using the VAX Debug facility. This allowed us to halt the program and

-- set the boom length to zero, eliminating the boom effects,

-- set the atmospheric density to the value found from previous SKYHOOK runs at the given altitude, 1.91×10^{-19} gm/cm^3,

-- set the drag "fudge factor" to 1.0

before the actual simulation.

Step 2: An input file for SKYHOOK was created and subsequently run. This was done by

-- starting with a typical equilibrium configuration input file as a model,

-- obtaining the initial vertical displacements and velocities of the "masses" relative to the Shuttle from the SLACK2 output and from internal SLACK2 variables examined with the debugger,

-- converting these to SKYHOOK initial conditions by
- adding the displacements to the Shuttle vertical coordinate
- scaling the horizontal velocities to give the same angular velocity as the Shuttle
- putting in the vertical velocity

-- setting the Shuttle mass to a high value (10^{15} gm) and area/mass low (0.36×10^{-10}) to approximate idealization in SLACK2,

-- setting the "subsatellite" mass and area/mass to the values for the final tether segment,

-- putting in a high tether elasticity, $E = 0.7 \times 10^{14}$, about a factor of 100 higher than Kevlar, to approximate the infinite E idealization of SLACK2 (higher values of E lead to SKYHOOK failure).

The case run in both programs corresponded to the following parameters (they were selected for this comparison only):

-- altitude 220 km, circular orbit
-- 0.2 cm diameter Kevlar tether
-- original 100 km tether deployed upwards with 0.3 ton subsatellite (determines recoil velocity)
-- tether broken 0.2 km from deployer
-- discretized to five tether segments (6 masses in SKYHOOK, including the Shuttle; 7 in SLACK2, with Shuttle and boom tip)
-- evolution followed for about 80 seconds.

Comparing and analyzing the resulting outputs is complicated by a variety of factors: the above mentioned disagreement in sign of the in-plane component; the presence of the deployment boom tip as an extra "mass" in the SLACK2 output; lack of a standard metric for comparing tether configurations. Development of the latter (perhaps a sum of squares of differences in mass position and/or differences in angles between segments) would be valuable for stability studies; but more intuitive considerations were adequate for the current comparisons, and highlighted many of the problems which had to be dealt with in early iterations. Three factors were considered separately: the general appearance of the configuration (side-view) plots; the vertical positions as a function of time; and the horizontal in-plane accelerations.

In-plane accelerations: This factor proved to be the most immediately diagnostic of differences between the models, leading to the corrections/allowances detailed above. The in-plane positions of the two end masses were extracted from the plot file using the printer plotter/lister. The resulting list of position as a function of time was then differenced twice to give acceleration (and the negative taken of SKYHOOK results).

In the initial period before any interactions, we expect a constant acceleration due to Coriolis forces and differential drag. This was indeed observed, and after discrepancies were identified and compensated for, the two programs gave identical accelerations: 1.20 cm/sec^2 in the forward direction.

Time history of vertical coordinates: The vertical ("radial") coordinates of the masses with respect to the Shuttle need no adjustment of sign and were plotted with the standard SKYHOOK post-processor for the results of both programs. These are shown in Figure K-1. Note that the SLACK2 results include a seventh mass, the boom tip, which is coincident with the Shuttle and hence has constant coordinate 0. The results are almost identical up until about T = 40 sec; after that they begin to diverge noticeably. Detailed examination of the printed results shows that this divergence coincides with a pair of nearly simultaneous bounces involving masses 3 and 2, then masses 2 and 1, between T = 40 and T = 41. The bounce times are printed explicitly by SLACK2 but must be inferred from the history of integration steps in the SKYHOOK output, the integrator taking very small steps near any discontinuity such as a change from slack to tensioned for any segment. For lower values of elasticity in SKYHOOK, these two bounces were reversed in order and the subsequent divergence was much more pronounced.

Configuration plots: A complete set of successive configurations at one second intervals is shown in the familiar in-plane vs. radial component side-view plot for the SKYHOOK results in Figure K-2. To allow a more detailed comparison of results we have plotted side-by-side the configurations of the SKYHOOK and SLACK2 results for several values of T in Figure K-3, appropriately inverting the SKYHOOK configurations to compensate for the different in-plane sign conventions. Results are in detailed agreement up to T = 40; reasonably good at T = 50; and agree only in a very general way thereafter. Of course, these are comparisons at the same time and do not rule out the possibility that the primary difference is simply a change or jump in the time scale, as can happen with

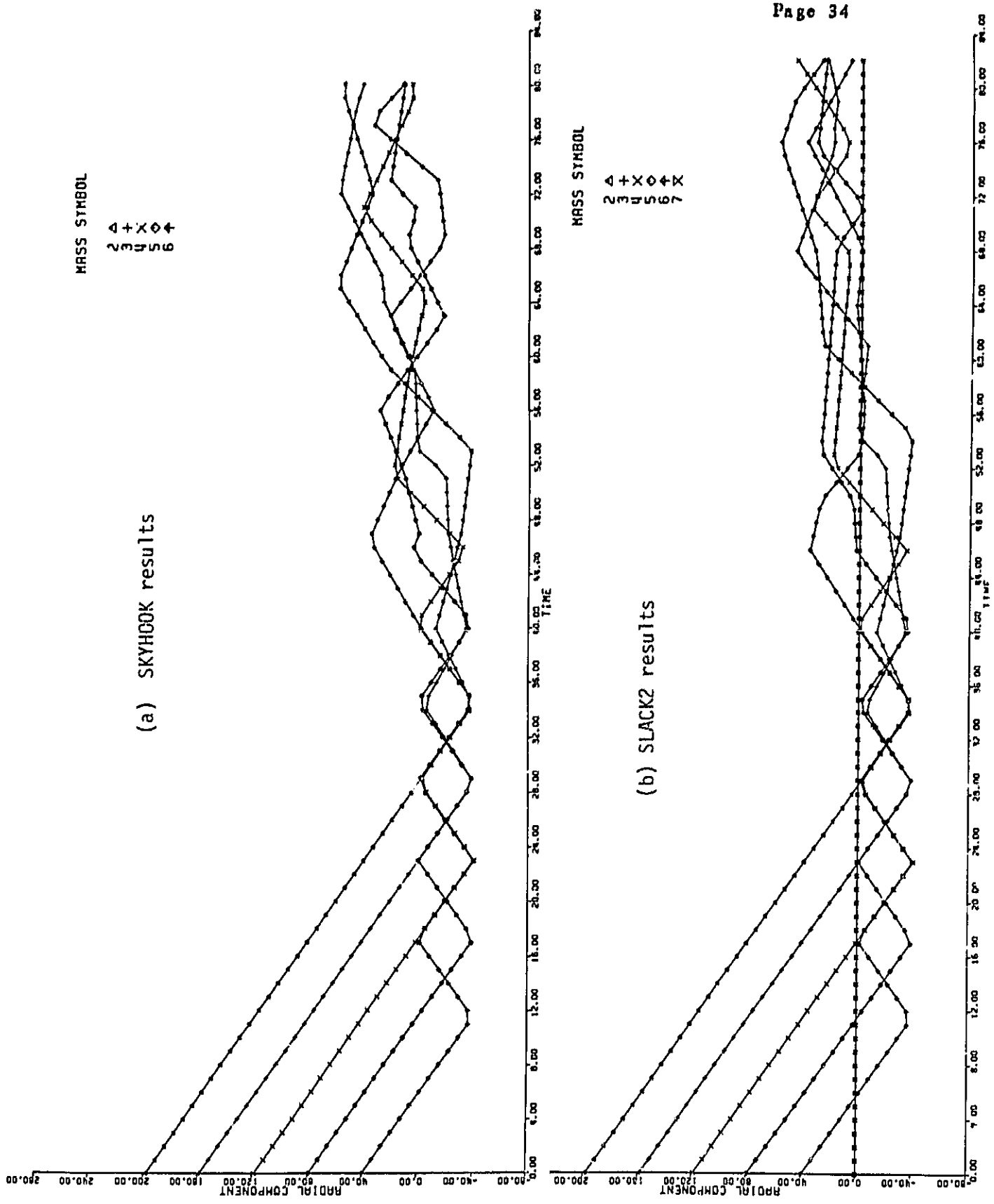

Figure K-1 - The radial components vs. time for (a) a SKYHOOK rum and (b) an equivalent SLACK2 run. See discussion in text.

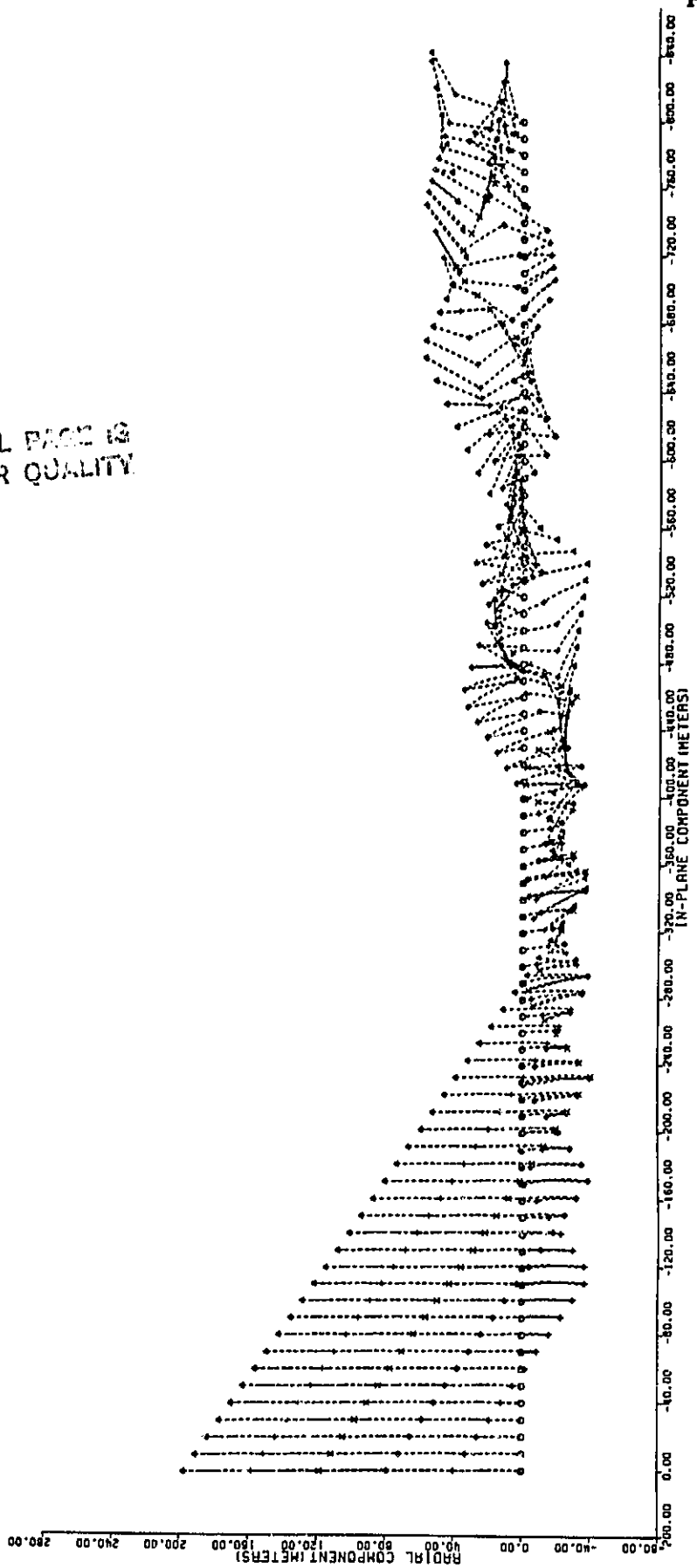

Figure K-2 - Successive configuration plots for the case considered in text (the SKYHOOK results are shown).

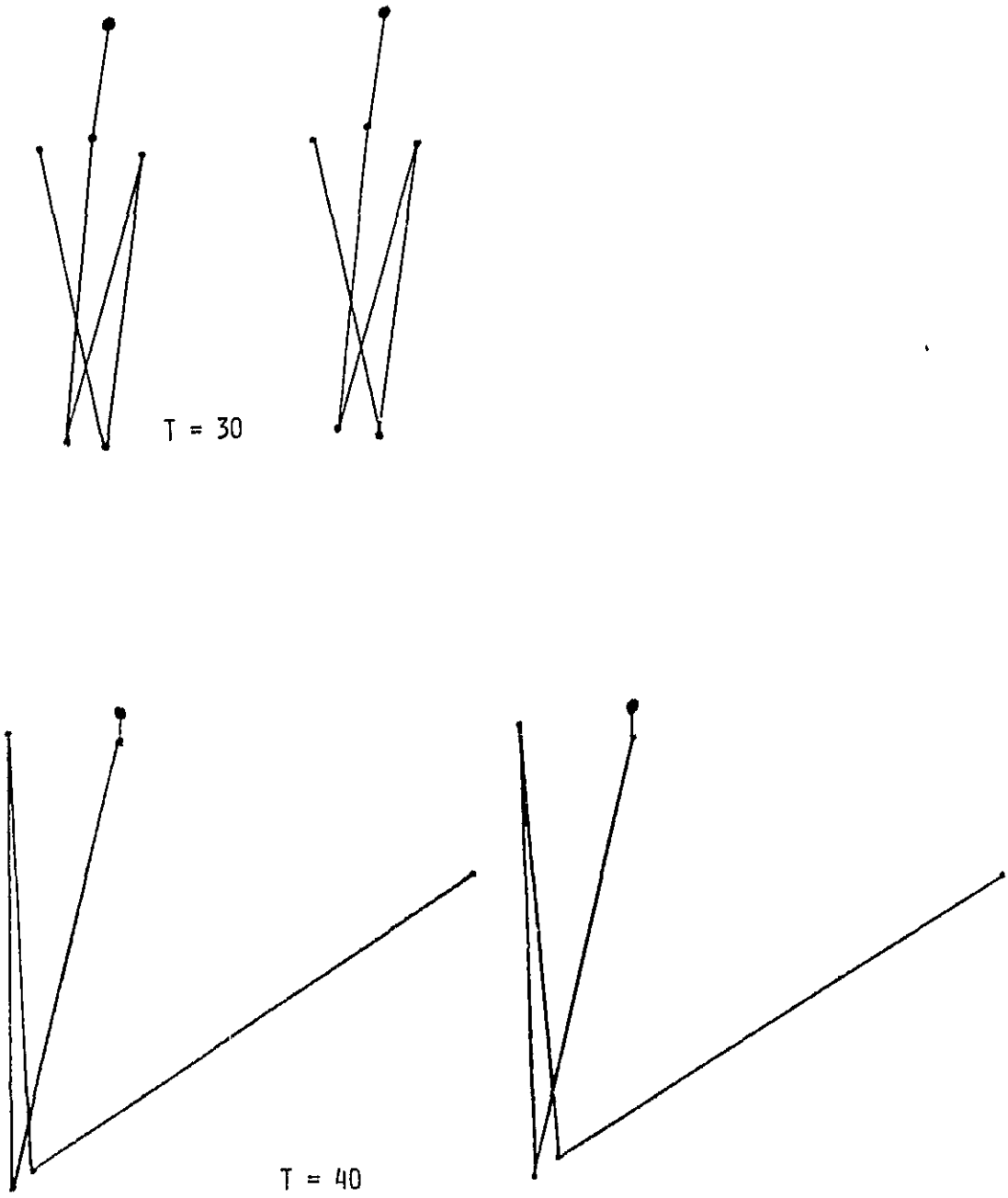

Figure K-3 - The configuration plots for SKYHOOK and SLACK2 simulation of the same case (as discussed in text) are shown side-by-side for several values of T. SKYHOOK results are on the left, inverted to make the in-plane components agree.

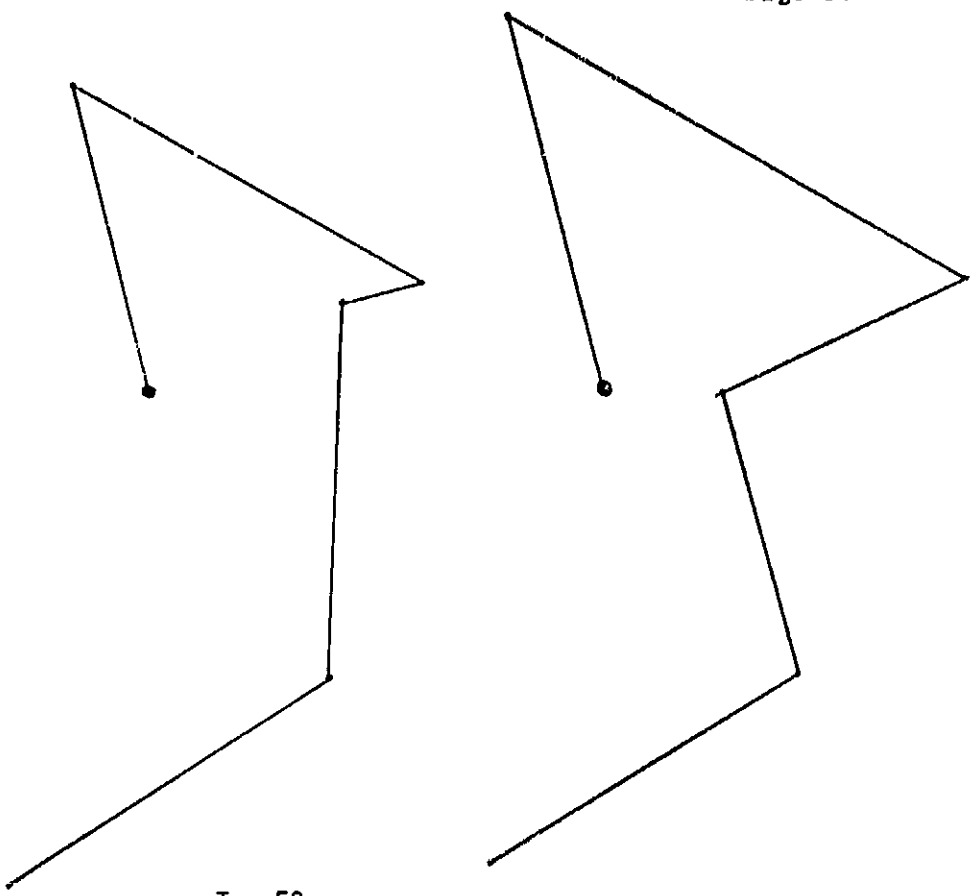

T = 50

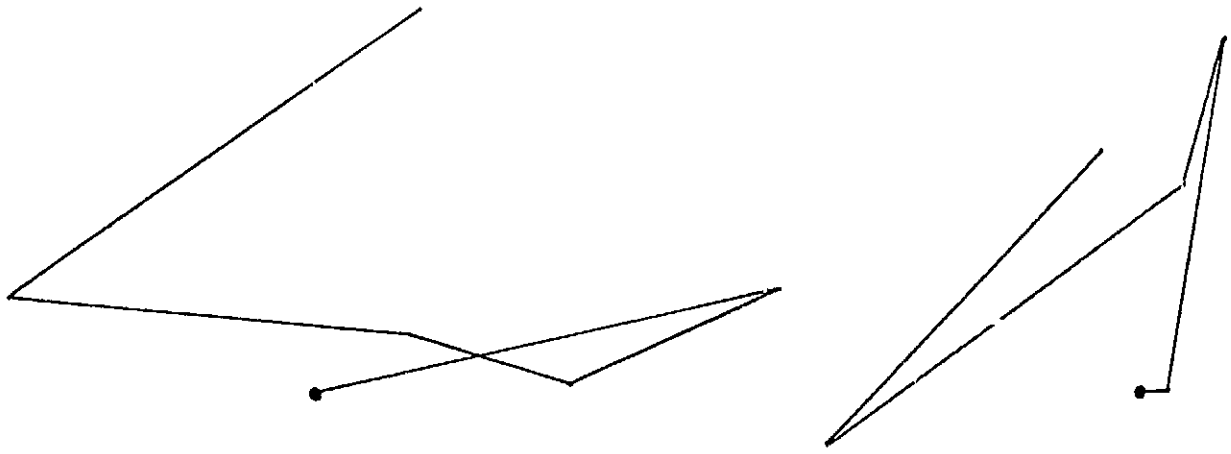

T = 60

Figure K-3

orbits: two particles in very close orbits will drift far apart if looked at simultaneously.

In summary, we may say that the agreement between SLACK2 and SKYHOOK is excellent once known differences are compensated for. These differences were intentionally chosen, in some cases representing extensions or corrections to SKYHOOK, in some cases for efficiency. The divergence in results after T = 40 sec is due more to the limitations of the overall "Ball and Spring" model than to problems with the SLACK2 program: the different results of the series of bounces between T = 40 and T = 41 could as easily have resulted from very slightly different initial conditions as from the slightly different treatment of bounces. This raises questions about the stability of the "Ball and Spring" model, and indeed of the actual physical system, which have only begun to be addressed.

2.2.3 Long Tether Remnants

In the SLACK2 model all free-flight forces are linear. Thus, when we start from the basic configuration of a set of masses traveling at the same velocity and separated by tether segments each slackened to the same degree (i.e. with separation the same fraction of natural length), all segments will come into tension simultaneously. When only a short length of tether remains after the break, interaction with the boom (to which the remnant is still affixed) disturbs the tether before the uniform lengthening can cause problems. Longer remnants, however, become taut before even the first mass is affected by the boom. Although SLACK2 can handle occasional nearly coincident bounces, there is no obvious algorithm for handling a case where several occur so as to interact: the program usually enters a broadly defined loop, bouncing the masses in some sequence over and over, or simply fails with some fatal error.

The method used to overcome this problem is to make the initial series of bounces non-simultaneous. This is done by introducing some randomization in the initial conditions. It is found experimentally that a few percent randomization in the slackness factor [separation/(natural length)] used for different segments, and one or two degrees randomization in the direction of the segments, is sufficient to prevent program failure. Figure K-4 shows results for a 100 km tether cut at 20 km, a case which previously could not be handled.

Typically there is a sharp burst of bounces when the tether initially tries to come into tension, the masses sort out their motions, and settle down to a regime of more normal bounce rates. E.g., in a case similar to that illustrated, there were no bounces until T = 66 sec, some 25 bounces until T = 69, 369 between T = 69 and 70, and thereafter a slow oscillation between a few bounces per second and a few tens of bounces per second.

2.2.4 Stability of the Lumped Mass Model

This resolution of our operational problem introduces seriously the questions about stability. In order to run at all, we must perturb the problem slightly; but do all such perturbations yield some identifiably similar end result, at least in the immediate aftermath of the initial burst of bounces? In general, for how long are simulations beginning with slightly perturbed results only slightly different? These questions also arose in the comparison of SKYHOOK and SLACK2 results, where the perturbation was to the details of the model rather than to initial conditions.

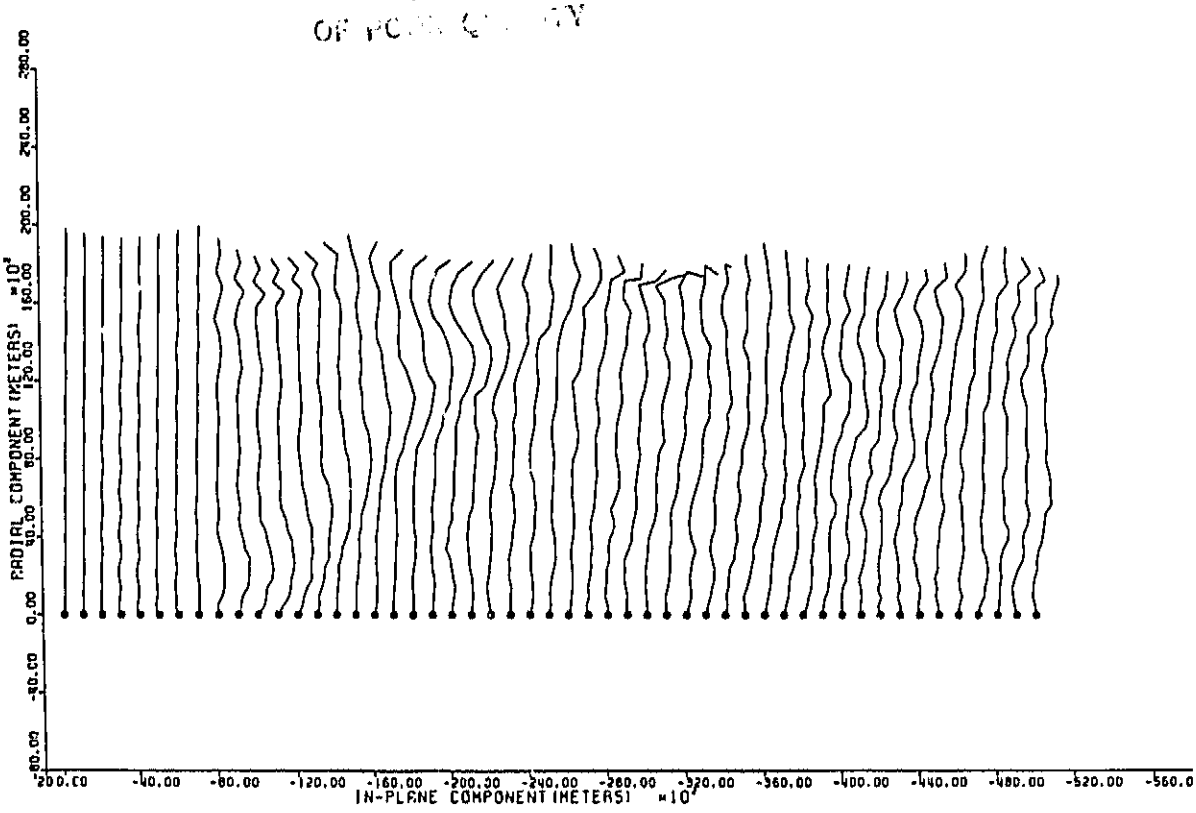

Figure K-4 - Results from a SLACK2 run with a long tether remnant after break (20 kilometers remaining from 100 km tether; 30 segments in simulation). This demonstrates that a small randomization of the initial conditions allows successful simulation in long remnant cases. Configurations are shown at 50 second intervals for 2500 seconds.

Investigations of a one-dimensional model, with no attachment point and only the gravity gradient force, were begun. Even a simple three-mass model leads to rapidly expanding numbers of special cases when studied analytically, before any significant results are obtained. We hope to program this model, perhaps on a microcomputer, and examine results of varying initial conditions.

2.2.5 Tether Longitudinal Damping

In this reporting period we used a crude damping feature that had been built into SLACK2 but not previously exercised.

Consider two masses and the connecting spring in their center of mass frame. If we assume a typical damping in the spring proportional to the rate of stretching, then each "bounce" (the one-sided spring becoming taut, stretching from the inertia of the masses, rebounding and becoming slack again) will result in a decrease of the masses' relative velocity by a constant fraction. This feature has been programmed into SLACK2 in that one inputs a "percent damping", e.g. 2% results in post-bounce velocity 0.98 times the pre-bounce velocity. This damping factor is applied uniformly to all segments regardless of length. (In the future we hope to investigate the appropriate physics so that we can input a physical quantity related to the tether material, and compute the appropriate damping factor for each segment.)

We shall use below a quantity we call the "retention". This is a simple approximation to the velocity we would expect to remain after a run, and is computed (post-hoc) as follows: count the number of bounces and divide by the number of segments to get the number of bounces per segment; if a segment were bouncing in isolation, after N bounces its velocity would be (damping factor)^N times the original, so we define this retention as

$$(\text{damping factor})^{[(\text{ bounces})/(\text{ segments})]}$$

A sequence of runs with different damping factors were made for the case:

-- original 20 km tether deployed upward with 0.5 ton subsatellite
-- cut at 0.2 km
-- boom deployed forward 30 degrees
-- discretized by 35 segments
-- evolution followed for 600 seconds.

The results are shown in Figure K-5 for damping factors of 0%, 0.5%, 1% and 2%; the resulting retentions were 1.00, 0.45, 0.14 and 0.02. The results of increased damping are about what one might expect: there is an overall decrease in the "crinkly" nature of the configurations and the effect of the vibrating boom becomes less apparent; the bouncing of the tether as a whole about the attachment point has longer period; and the effects of drag become more pronounced. An unexpected feature is that the first excursion past the attachment point is <u>further</u> the greater the damping; the boom seems to retain some tether in its vicinity in the undamped case.

The 2% damping case was followed for a longer period, 3000 seconds. The results are shown in Figure K-6. Note that the tether appears to be oscillating about a "downwind" dragging position. With the "balloon" drag model used, and approximating the tether as a single mass, this downwind configuration can be shown to be stable for tethers less than about a kilometer long. The retention factor for this run is extremely small: $(0.98)^{[(19058 \text{ bounces})/(35 \text{ segments})]} = 2 \times 10^{-5}$. One would expect to see a perfectly motionless system, but instead the tether is obviously still moving moderately briskly at least. Possible sources of energy input are

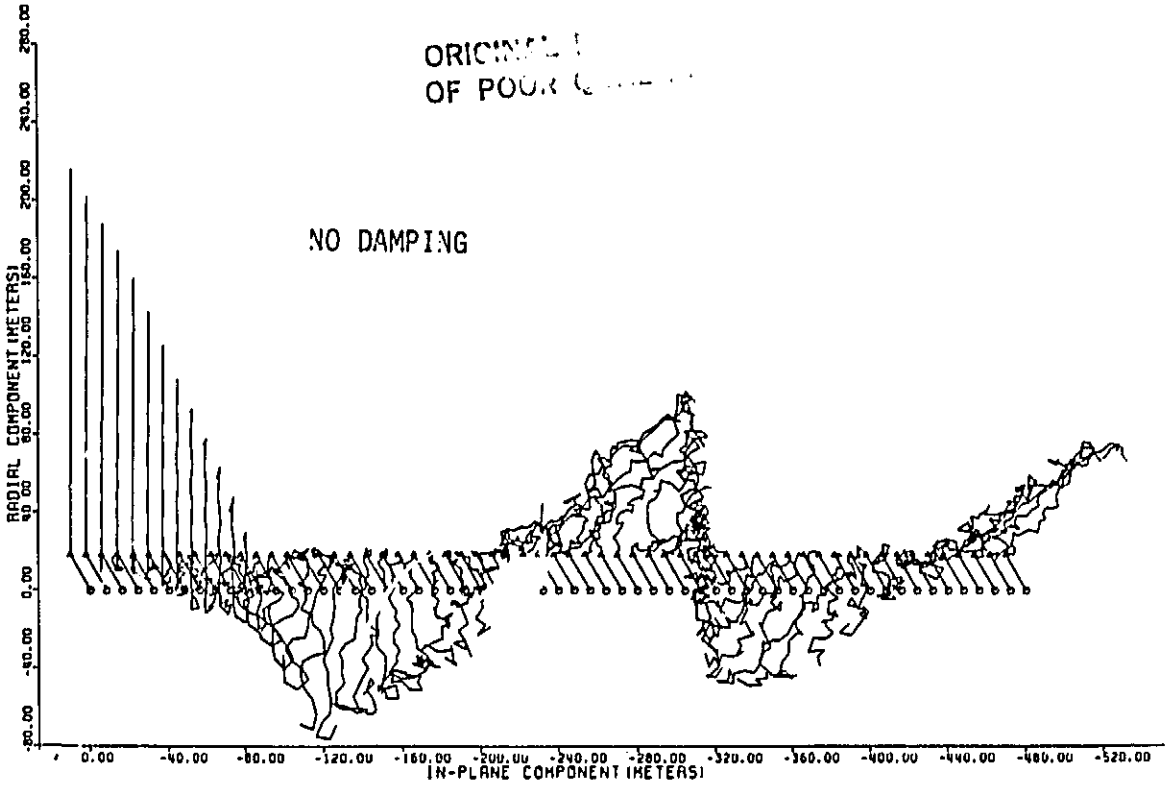

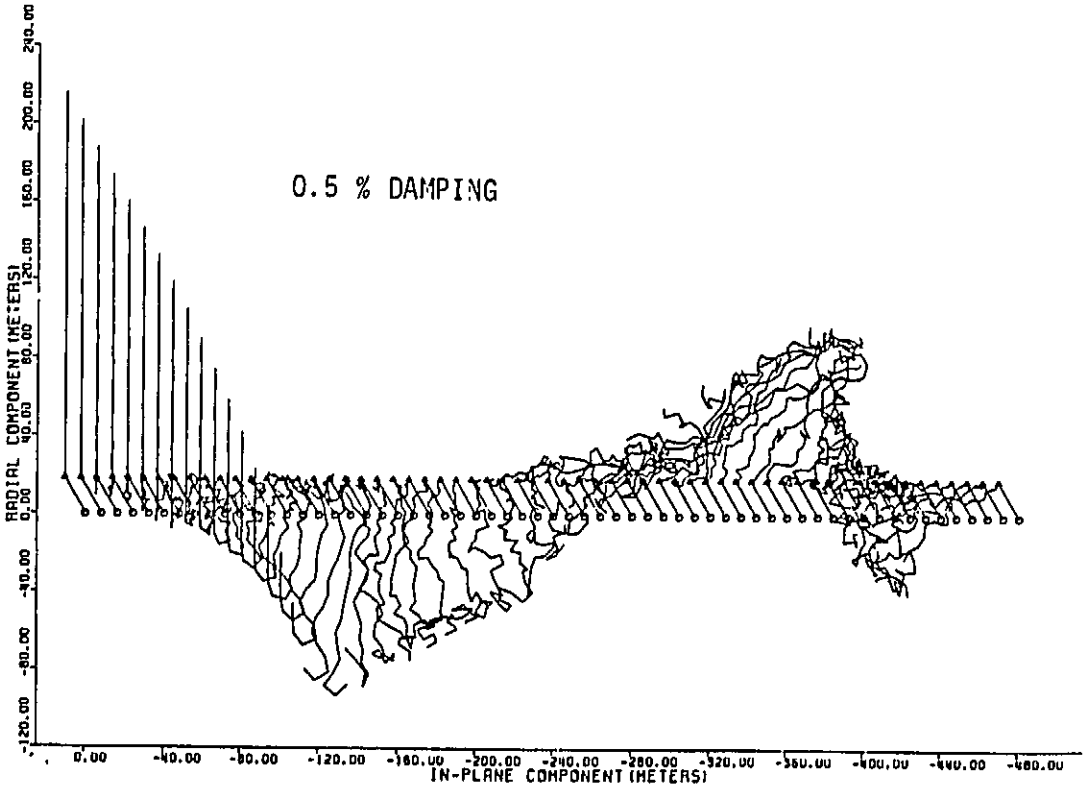

Figure K-5 - SLACK2 results for a sequence of runs in which only the tether damping varies. Otherwise, the cases are all the same: 0.2 km remaining from a 20 km upward deployed tether: 35 segment discretization; 600 second simulation with output at 10 second intervals. Damping factors of 0%, 0.5%, 1% and 2% are used, as discussed in the text.

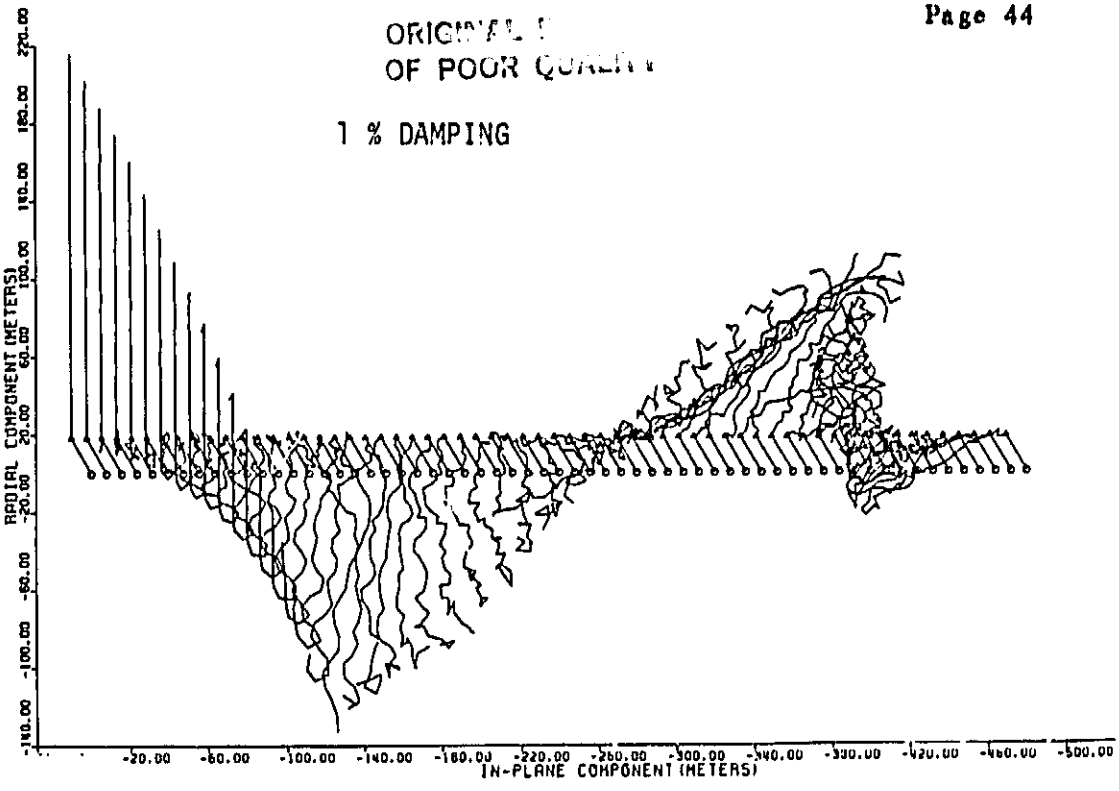

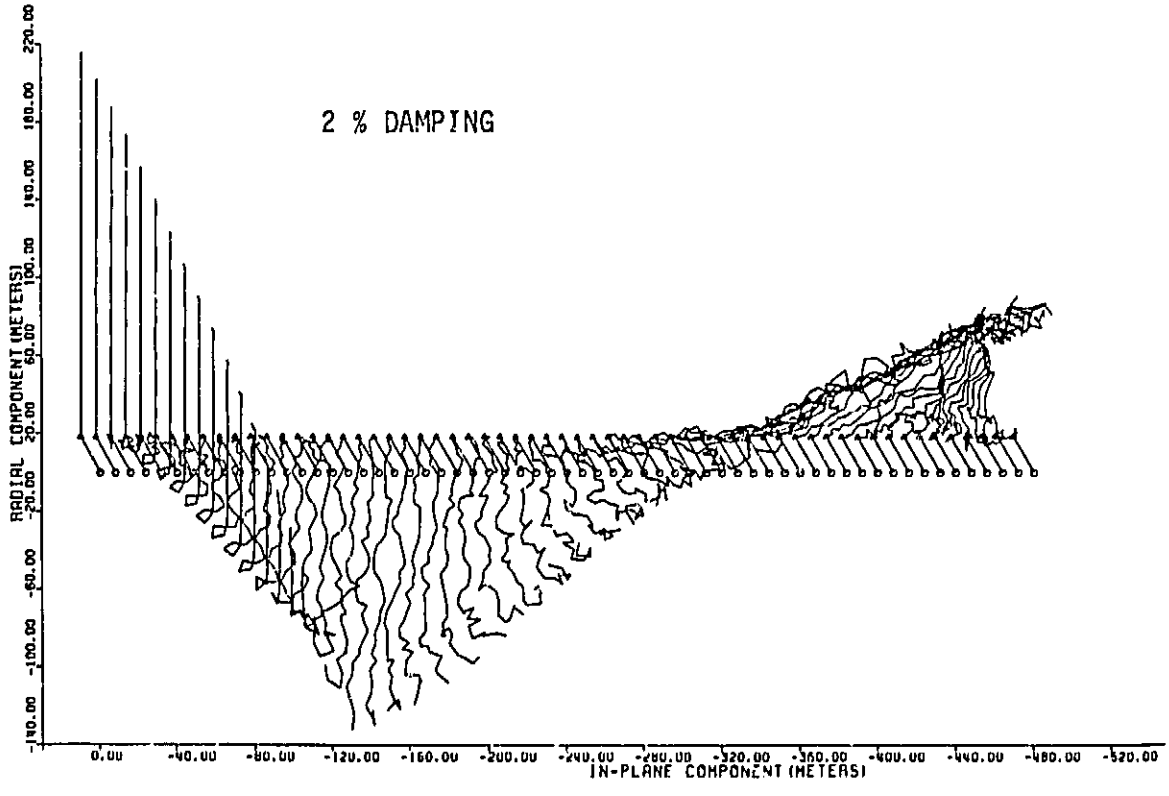

Figure K-5

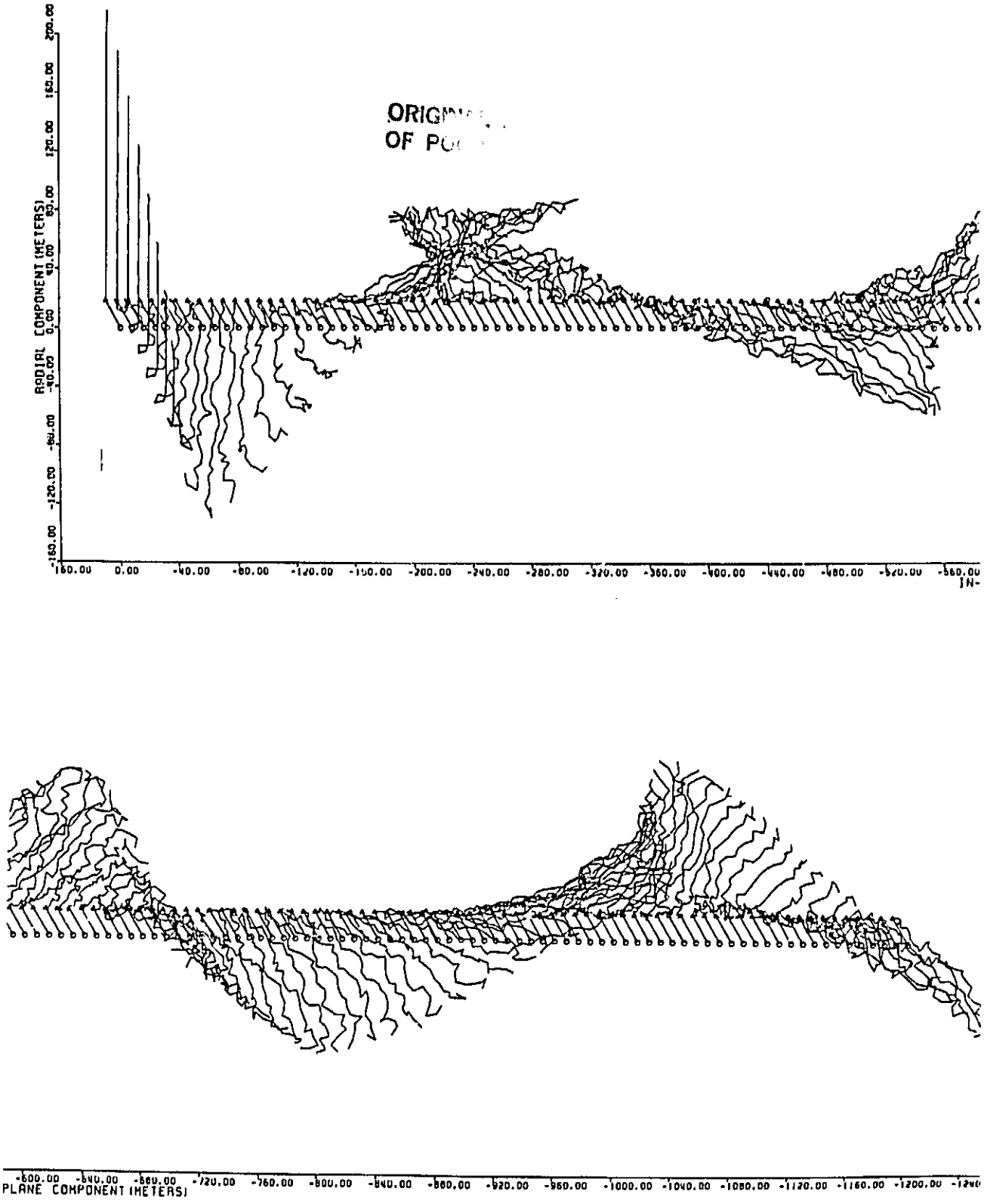

Figure K-6 - The final case of Figure K-5 (2% damping) is followed for 3000 seconds, showing configurations at 20 second intervals.

air drag and the vibrating boom. It would be of interest to compute the total kinetic energy as a function of time; we might expect this to show an initial decrease due to damping but eventually reach an equilibrium between damping and forcing.

We should point out that under the influence of damping the "almost always slack" model used must eventually break down. In a real tether, the gravity gradient and/or drag forces will eventually bring the tether into constant tension, unless there is some disturbing influence such as the vibrating boom. How will SLACK2 respond to this challenge? A run with a non-vibrating boom should be made, but one may make a theoretical prediction as well: If one analyzes the simplest case of one tether mass and an infinite mass Shuttle with only the gravity gradient force applying, one finds that the velocity reduction at each bounce causes the time to the next bounce to be reduced by the same ratio. Thus, as the system approaches tension, the bounces become infinitesimally spaced and approach a constant time. We have not seen this directly in the SLACK2 runs because of the booms energy input.

2.2.6 References

Colombo, G., Arnold, D.A., Gullahorn, G.E. and Taylor, R.S., 1984. "Investigation of Electrodynamic Stabilization and Control of Long Orbiting Tethers," Final Report on Contract NAS8-35036.

Gullahorn, G.E., 1983. "Slack Tether: High Resolution, Two Dimensional Model," technical appendix to Monthly Progress Report #11, Contract NAS8-35036 (G. Colombo, PI).

2.3 Preliminary Analysis of Electro-Mechanical Failures and Tentative Assessment of the Related Consequences

2.3.1 Introduction

The electrodynamic tethers that will be flown in the forthcoming first and third demonstration flights of the Shuttle-borne TSS facility could, in principle, represent safety hazards due to the high-voltage electro-motive force that they will generate. In this preliminary analysis we show that these hazards are not too worrisome. Thus far, however, we have limited our investigation to the hazards to be expected from possible failures occurring while the 20 km tether is fully deployed (upwards). Before the occurrence of failures, the lower end of the tether is assumed to be connected to the Shuttle and the Shuttle is assumed to be kept at the plasma potential by a suitable plasma contactor (hollow-cathode plasma bridge). The upper end of the tether is assumed connected to the subsatellite. Two different situations are assumed for the latter: (1) presence, and (2) absence of a plasma contactor.

The main failure modes are the following:

1) Malfunction of the Shuttle-borne plasma contactors;

2) Malfunction of the plasma contactor in the subsatellite (when such a plasma device is present);

3) Breakage of the tether (either near the upper end, or in the middle, or near the lower end).

The simplified diagram of the electrodynamic tether system is given in Figure L. For a 20 km tether, the electromotive force (emf) has an orbital average of 3.78 KV, for a typical 28° orbital inclination and a 295 km orbital height. The contact resistances R_1 and R_2 are of the order of 1Ω,

when plasma contactors are used at both tether's ends, and when they function properly. The resistance of the ionospheric closure circuit R_{iono} is also of the order of 1 ohm. Present plans for the 20 km wire call either for R_W = 1,686 kΩ (25.7 ohm/1000 ft) or for 4k Ω (.2 ohm/m). We assume here that R_L is also equal to either 1,686 Ω, or 4000 Ω.

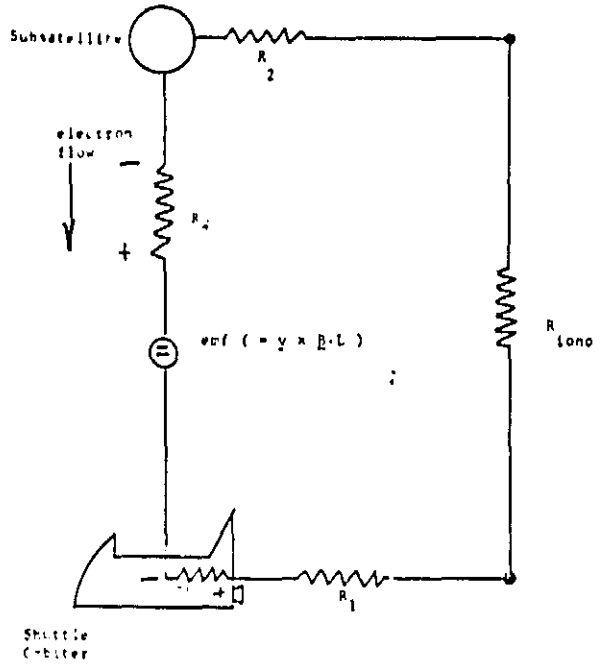

Fig. L Simplified equivalent circuit of electrodynamic tether (tether deployed upwards, shuttle in eastward motion).

Consequently, for a 1.686 kohm tether the current I_W in the wire is expected to be about I_W = 1.12 A, with 2118.6 watts dissipated in the tethers ohmic resistance and an equal 2118.6 watts dissipated in the on-board loads. In fact, when plasma contactors are used at both ends of the tether, a current intensity I_W = 1.12 A is well with feasibility. On the contrary, when plasma contactors are used solely on the Shuttle Orbiter, the current I_W in the wire is limited by the charge-capture capability of the terminating subsatellite (a metal sphere with diameter = 1.5 m). This upper limit for the current has been computed to be I_W = 0.63 A.

2.3.2 Consequences of Plasma Contactor Failure

If plasma contactors are used at both ends of the tether, failure of one of them will have as a consequence the appearance of a high potential between that termination where the hollow-cathode plasma contactor failed, and the surrounding medium. Let's consider the case of hollow-cathode failure on-board the tethered subsatellite. When this occurs, the "contact" with the ionosphere is provided now solely by the metal skin of the 1.5 m diameter spherical subsatellite. We have already indicated that the current I_W will drop from 1.12 A to 0.63 A. The resistance R_1 of the equivalent circuit (see Figure L) has now increased in value from about 1 ohm to 2,628 Ω. A difference of potential + 0.63 x 2628 = +1665.6 volt is established between the external surface of the subsatellite and the plasma environment. This potential is highly superthermal and we should not expect that its distribution around the subsatellite will follow the prediction of quiescent plasma sheath theory. It is more likely that, owing to collective effects, the perturbed volume will be larger than predicted and will resemble some sort of "corona discharge" with accelerated plasma populations inside. Hazards, deriving from this situation do not seem, however, to be worrisome. It is more probable that we will have here the opportunity of performing interesting plasma physics measurements, rather than experiencing damages to the subsatellite instrumentation. The risk at least seem affordable. Instead, a serious hazard is represented by the possibility that the Shuttle-based hollow-cathodes may fail, thus leaving the electric potential of the Shuttle free to increase from such a safe operational values as a few volts (negative) to very high negative values with respect to the surrounding medium. An initial calculation (to be verified in next reporting period)

performed by assuming that the upper end of the tether is terminated by a 1.5m diameter subsatellite without plasma contactor, has indicated that the negative voltage acquired by the Shuttle in case of failure of the Shuttle-mounted hollow-cathode is about -2kv with respect to the environment plasma.

We plan to perform in the forthcoming contract's performance period detailed calculations of the potentials acquired by each tether's end in case of failure of plasma contactors. It is already obvious, however, that a hollow-cathode failure at the Shuttle end would have serious consequences. Provisions must be taken (by use of a redundant arrangement of several hollow-cathode devices in parallel, or by some other approach) to reduce as much as possible the probability of the occurrence of such an event. It would also appear that, in order to alleviate at least in part the consequence of the failure of the Shuttle-mounted hollow-cathodes, the plasma contactor on-board the subsatellite should be switched off by the operator. This would make it possible to localize part of the excess difference of potential at the subsatellite end of the tether (where it is less worrisome) thus reducing the negative voltage acquired by the Shuttle Orbiter with respect to the plasma medium.

2.3.3 Consequences of Wire Breakage

2.3.3.1 General

In all the analytical efforts that have been performed thus far on the electrodynamic interactions between the ionospheric medium and an insulated metallic tether with terminating electrodes, the assumption always has been that the typical dimension of such electrodes are greater than the electron Debye length λ_d. At the orbital altitude of the TSS demonstration flights, λ_d = 3 to 5 mm. This condition is amply met when the free end of the wire is terminated by a subsatellite. This is however no more so, when a wire breakage occurs. In this case a high potential could appear between the small dimension, truncated tether's tip and the surrounding medium. A first-cut estimate of the extent of this high potential was performed by Olbert (1983), who modelled the long tether as an elongated prolate spheroid in vacuo. Olbert's approach would lead to values of the electric field near to the truncated tip of the wire that would be high enough to be worrisome. However Harrold (1984) has shown that we can realistically expect there lower values for the electric field.

Section 2.3.3.2 of this report illustrates Olbert's approach, while Section 2.3.3.3 contains Harrold's revision and his estimate of the expected values of the electric field near the tip of the truncated wire, at various distances from the wire's tip.

2.3.3.2 Olbert's Method of Computation and Numerical Results

As already pointed out in the previous Section, Olbert (1983) modelled the long wire as an elongated prolate spheroid vacuo. His computation of the electric field near the truncated tip of the wire proceeds as follows. With reference to Figure M, the electric field E_n at the point of the wire that is at a distance y from the tether's mid point is given by the expression

$$|E_n| = \frac{y\ a^2 E_\infty}{Q_1 b \sqrt{a^4 - (a^2 - b^2) y^2}} \qquad (1)$$

where (see Figure M for definition of a, b):

E_∞ = field at infinity = $|\bar{V} \times \bar{B}|$

a = tether length (after breakage)

b = wire's radius = 10^{-3}m

Q_1 = $\ln\left(\frac{2a}{b}\right) - 1$.

The highest value $E_{n\,(max)}$ occurs when y = a. In this case, equation (1) yields:

$$E_{n\,(max)} = \frac{a^2\ E_\infty}{b^2\ Q_1} \qquad (2)$$

Because, in our case $E_\infty = |\bar{V} \times \bar{B}| \simeq 0.189$ V/m, we obtain from (2)

$$E_{n\,(max)} = \frac{a^2}{b^2 Q_1} \times 0.189\ \frac{V}{m}$$

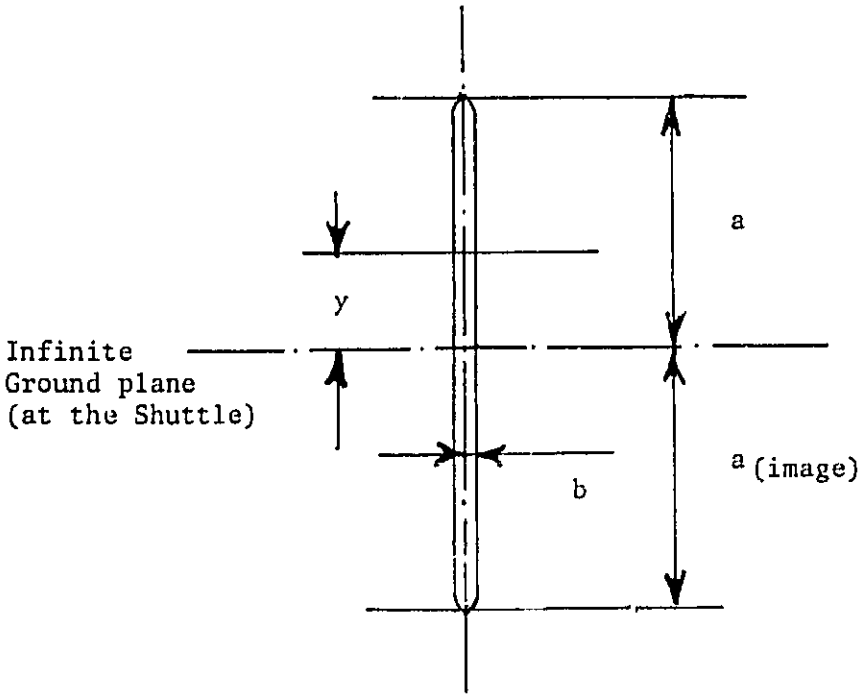

a = semimajor axis of equivalent prolate spheroid = 2×10^4m

b = Semiminor axis

Figure M

In-vacuo, elongated prolate spheroid model of long orbiting tether

Let's examine the following cases:

1. Wire breakage at attachment point to subsatellite (20 km above Shuttle):

$a = 2 \times 10^4$ m

$Q_1 = 16.5$

$$E_{n(max)} = \frac{4 \times 10^8}{10^{-6} \times 16.5} E_\infty = 4.5 \times 10^{12} \text{ V/m (at truncated end)}$$

2. Wire breakage, 2 km above the Shuttle:

$a = 2 \times 10^3$ m

$Q_1 = 14.2$

$$E_{n(max)} = \frac{4 \times 10^6}{10^{-6} \times 14.2} E_\infty = 5.3 \times 10^{10} \text{ V/m (at truncated end)}$$

3. Wire breakage, 200 m above the Shuttle:

$a = 2 \times 10^2$ m

$Q_1 = 11.899$

$$E_{n(max)} = \frac{4 \times 10^4}{10^{-6} \times 11.899} E_\infty = 6.3 \times 10^8 \text{ V/m (at truncated end)}$$

4. Wire breakage, 20 m above Shuttle:

$a = 20$m

$Q_1 = 9.5966$

$$E_{n(max)} = \frac{4 \times 10^2}{10^{-6} \times 9.5966} E_\infty = 7.9 \times 10^6 \text{ V/m (at truncated end)}$$

5. Wire breakage, 2 m above Shuttle:

$a = 2$m

$Q_1 = 7.29$

$$E_{n(max)} = \frac{4}{10^{-6} \times 7.29} E_\infty = 1.03 \times 10^5 \text{ V/m (at truncated end)}$$

***

2.3.3.3 Revision of Olbert's Approach*

2.3.3.3.1 Introductory Remarks

The electric field in the vicinity of a wire travelling through a uniform magnetic field B can be calculated from the approximation that at velocities much smaller than the velocity of light, the Lorentz transformation states that the wire is immersed in a uniform electric field

$$\vec{E} = \vec{V} \times \vec{B} \qquad (3)$$

As viewed by an observer travelling with the wire.

One approach to the calculation of the distortion of the otherwise uniform $\vec{E}$ field is to model the wire as a long slender prolate spheroid (Olbert, 1983). It will be shown here that while this model is reasonable at some distance from the ends of the wire it is very inaccurate close to those ends.

The electric field calculated at the end of the wire, by the Olbert's method is on the order of a teravolt/meter. Even if this erroneous result were correct, it will be shown in this section that the electric field, one meter from the end of the wire, would already be down to 114.64 volts/meter.

The assumptions made for the calculations carried out in this section are as follows:

---

*Contributed by W.J. Harrold (see reference Harrold, 1984, in Section 2.3.3.3.6)

a - length of wire 20 km

b - diameter of wire 2 mm

c - one end of wire attached to a large conducting spacecraft (Shuttle Orbiter)

d - prolate spheroid model

--semi major-axis $a = 2 \times 10^4$ m

--semi minor-axis $b = 1$ mm

e - spacecraft modelled as an infinite ground plane so that the tether length is doubled and therefore $a = 2 \times 10^4$ m

2.3.3.3.2 Prolate Spheroid Model

It can be shown that the electric field on the axis of a dielectric spheroid, of dielectric constant K, immersed in a uniform field E_o is given by

$$E_n = E_z = C_1 \left[Q_o(\xi) - \frac{\xi}{\xi^2-1}\right] - E_o, \quad z>a \tag{4}$$

where:

$$\xi = z/c \tag{5}$$

z = the distance from the center of the spheroid (meters)

C = the semi-focal length of the spheroid $C^2 = a^2 - b^2$

a = the semi-major axis

b = the semi-minor axis

$$Q_o = \frac{1}{2} \ln \left(\frac{\xi+1}{\xi-1} \right) \tag{6}$$

and:

$$C_1 = \frac{\xi_o E_o}{Q_1(\xi_o) + 1/[(k-1)(\xi^2-1)]} \tag{7}$$

where:

$$\xi_o = a/c \tag{8}$$

and:

$$Q_1(\xi) = Q_o(\xi) - 1 \tag{9}$$

The function $Q_o(\xi)$ and $Q_o(\xi)$ are the zeroth and first degree legendre functions of the second kind of order o.

One can calculate the field around a conducting spheroid by taking the limit as $k \to \infty$ thus:

$$\lim_{k \to \infty} C_1 = \frac{\xi_o E_o}{Q_1(\xi_o)} \tag{10}$$

2.3.3.3.3 Electric Field at the End of the Spheroid

We substitute (10) into (4) for $\xi = \xi_o$ and find that

$$E_\eta = \frac{\xi_o E_o}{Q_1(\xi_o)} \left[Q_o(\xi_o) - \frac{\xi_o}{\xi_o^2 - 1} \right] - E_o$$

$$= \frac{E_o}{Q_1(\xi_o)} \left[Q_1(\xi_o) + 1 - \frac{\xi_o^2}{\xi_o^2 - 1} \right] - E_o \qquad (11)$$

$$= \frac{E_o}{Q_1(\xi_o)} \left[Q_1(\xi_o) - \frac{1}{\xi_o^2 - 1} \right] - E_o$$

$$= \frac{-E_o}{(\xi_o^2 - 1) Q_1(\xi_o)} \qquad (12)$$

An approximate calculation of $Q_1(\xi_o)$ can be performed as follows:

$$Q_1(\xi_o) = \frac{\xi_o}{2} \ln \left(\frac{\xi_o + 1}{\xi_o - 1} \right) - 1 \qquad (13)$$

where:

$$\xi_o = a/c$$

Therefore:

$$Q_1(\xi_o) = \frac{\xi_o}{2} \ln \left(\frac{a+c}{a-c} \right) - 1 \qquad (14)$$

where:

$$c = \sqrt{a^2 - b^2} \qquad (15)$$

$$c = a\sqrt{1 - \left(\frac{b}{a}\right)^2} \qquad (16)$$

and:

$$\frac{b}{a} = 10^{-3} / 2 \times 10^{4} = 5 \times 10^{-8}$$

Therefore C is closely approximated by:

$$c = a[1 - \frac{1}{2}(\frac{b}{a})^2]$$

$$= a - \frac{b^2}{2a}$$

and

$$a - c = \frac{b^2}{2a} \tag{17}$$

Thus:

$$\ln(\frac{a+c}{a-c}) = \ln(\frac{2a}{b^2/2a}) = 2\ln(\frac{2a}{b}) \tag{18}$$

Substituting this result into (13) we find that:

$$Q_1(\xi_o) = \frac{a}{c}\ln(\frac{2a}{b}) - 1 \simeq \ln(\frac{2a}{b}) - 1 \tag{19}$$

Furthermore we find that:

$$\xi_o^2 - 1 = \frac{a^2}{c^2} - 1 \simeq \frac{b^2}{a^2} \tag{20}$$

We now substitute (19) and (20) into (11) with the result:

$$|E_{\eta_o}| = \frac{a^2|E_o|}{b^2[\ln(\frac{2a}{b}) - 1]} = 4.5 \times 10^{12} \text{ V/m} \tag{21}$$

in agreement with Olbert (1983) [see equation (2) in Section 3.2].

2.3.3.3.4 Calculation of the Electric Field on the Axis of the Prolate Spheroid

The results of the previous section would like worrisome, if we do not check how small is the region where the electric field is so high. A computer program was written to calculate E_η as a function of $(z - a)$. A summary of these results is given in Table I, hereunder (see Figure N).

Table I

Values of the Electric Field on the axis of the prolate Spheroid at Various Distances from the Tip

$(z - a)$	$\lvert E_z \rvert$ V/m
10^{-10} m (1 A)	1.1451×10^{12}
10^{-9} m (10 A)	1.1451×10^{11}
10^{-8} m (100 A)	1.1451×10^{10}
10^{-7} m (1000 A)	1.1451×10^{9}
10^{-6} m (1μ)	1.1451×10^{8}
10^{-5} m (10μ)	1.1451×10^{7}
10^{-4} m (100μ)	1.1452×10^{6}
10^{-3} m (1 mm)	1.1452×10^{5}
10^{-2} m (1 cm)	1.1453×10^{4}
10^{-1} m (10 cm)	1.1453×10^{3}
1 m	114.64
10 m	11.59
100 m	1.30
1 km	0.28

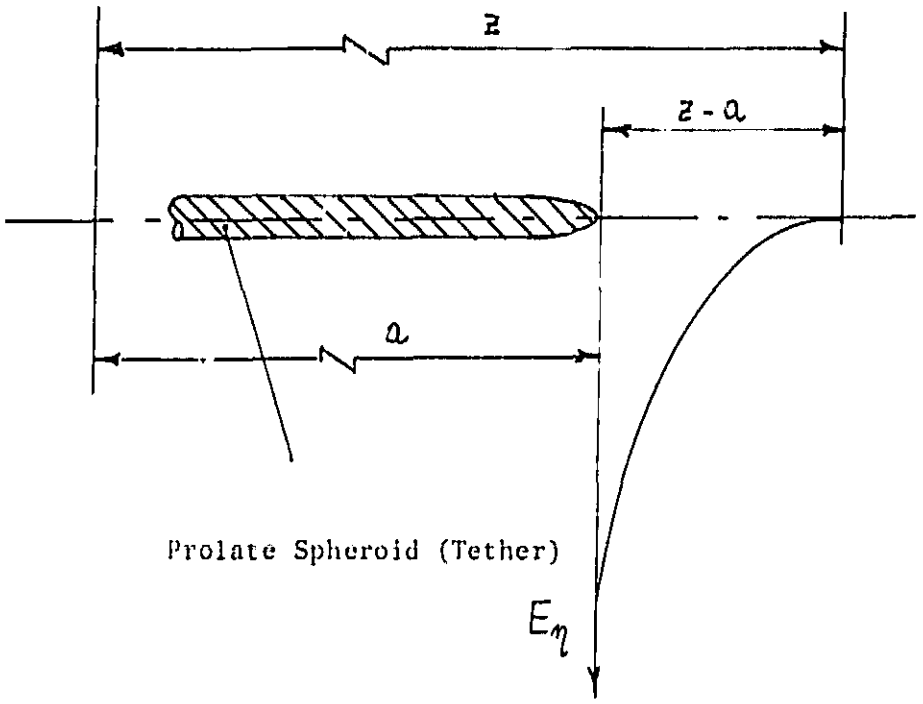

Figure N - Geometry for Electric Field Computation (figure not to scale).

2.3.3.3.5 Demonstration that the Near-Field of the Prolate Spheroid is an Incorrect Model

The radius of curvature of a curve is given by the reciprocal of the second derivative. For example in the case of the circle:

$$x^2 + y^2 = R^2$$

$$y = (R^2 - x^2)^{1/2}$$

$$\frac{dy}{dx} = \frac{-x}{\sqrt{R^2-x^2}}$$

$$\frac{d^2y}{dx^2} = \frac{-1}{\sqrt{R^2-x^2}} - \frac{x^2}{(R^2-x^2)^{3/2}}$$

At $x = 0$:

$$\frac{d^2y}{dx^2} = \frac{\pm 1}{R}$$

The spheroid analyzed in this section is a result of rotating the ellipse defined by:

$$\frac{x^2}{a^2} + \frac{y^2}{b^2} = 1$$

About its major axis "2a"

$$x = a\sqrt{1 - y^2/b^2}$$

$$\frac{dx}{dy} = - y \frac{a}{b^2} \left(1 - \frac{y^2}{b^2}\right)^{-1/2}$$

$$\frac{d^2x}{dy^2} = \frac{-a}{b^2\sqrt{1 - y^2/b^2}} + \frac{y^2 a}{b^4} \left(1 - \frac{y^2}{b^2}\right)^{-3/2}$$

At y = 0:

$$\frac{d^2y}{dy^2} = -\frac{a}{b^2}$$

or:

$$R = \frac{b^2}{a} = 5 \times 10^{-11} \text{ m}$$

Since the radius of the wire is b we find that the radius of the sharp end is too small by a factor of b/a or 5×10^{-8}.

The voltage at the surface of a charged sphere can be computed as follows. The electric field of a charge q is given by

$$E_r = \frac{q}{4\pi r^2 E_o}$$

The potential at a radius r, is given by:

$$V_{r1} = \int_{r1}^{\infty} \frac{q\, dr}{4\pi r^2 E_o} = \frac{q}{4\pi r_1 E_o}$$

Thus:

$$q = 4\pi r_1 V_{r1} E_o$$

and:

$$E_{r1} = \frac{V_{r1}}{r_1}$$

If r_1 is erroneously calculated to be too small by the factor 2×10^7 then the electric field at that miniscule radius will be too high by the factor 2×10^7.

2.3.3.3.6 Concluding Remarks

We have calculated the electric field at the end of a prolate spheroid moving in a uniform magnetic field and we have shown that this model (Olbert, 1983) gives electric fields which are too high by a factor of 20 million. We have also shown that, even if one accepts the predictions of the spheroidal model, the electric field strength drops to 114.64 volts/meter at a distance of one meter from the end of the spheroid.

Thus far, our analysis has not disclosed electric hazards that are serious enough to require some changes in NASA plans for the two electrodynamic tether missions of 1987-1990. We will continue, though, in our search, especially in connection with slack-tether situations that might bring the truncated tip of the wire (with corona discharges around it) close to the Shuttle Orbiter.

2.3.3.3.7 References

Harrold, J.W., 1984. Calculation of the electric field strength at the end of a wire travelling in vacuo with respect to a uniform magnetic field, SAO Technical Note TP84-V, November 19.

Olbert, S., 1983. The electrodynamic tether. Seminar given at MIT Center for Space Research, November 1.

2.4 Program Status of the TSS Rotational Dynamics Model

The modelling of the external perturbations affecting the rotational dynamics of the satellite has been started. The implementation in the computer code has not yet been done so that presently the crude original version is the only one running. With regards to the external perturbations this version models the tension only, and it is therefore suitable for first approximation simulation. We are also working on the analytical formulation of the rigid body motion that presently integrates the nine directions cosine along with the three rigid body equations of the satellite. The idea is to derive the expressions of the satellite rotational velocities, P, Q, R (in body axis) as a direct function of the Euler's rotational velocities. This strategy will decrease the total number of equations for the rigid body rotation of the satellite from 12 to 6. The disadvantage is to have a singularity at the equation describing the roll motion for a roll angle of 90 degree from the local vertical. Such value however represents a limit condition. First results of the up-dated rotational dynamics model will be presented in the next quarterly report.

2.5 Problems Encountered During Reporting Period

None

2.6 Activity Planned for the Next Reporting Period

The activity on the out-of-plane dynamics during the first electrodynamic mission (it was extended to the out-of-plane oscillation damping issue and to an accurate estimation of the tether bowing) is to be considered complete unless otherwise directed by NASA/MSFC.

In the area of high resolution slack tether studies, the SLACK2 computer code will be soon available in its three dimensional formulation. We will start to simulate dynamics after the break in the most critical conditions (we look for inputs from NASA/MSFC). The study of the slack tether will be linked as far as possible to the electrodynamic hazard investigation.

In this area we plan to continue our analysis of the effects of the plasma contactor's failure, and to perform detailed calculations, using the SKYHOOK code, of the voltages acquired, because of this failure, by each tether's end, with respect to the medium.

In addition, we plan to analyze further the wire breakage cases. For these, we will construct an improved model of the truncated wire and with this new model we will replace the elongated prolate spheroid that we found to be inadequate. In addition, we will start the development of an approach for the evaluation of the effects of ionospheric plasma on the strength of the electric field in the vicinity of the truncated tip.

The up-grade of the rotational dynamics model will be completed with the modelization of the major external perturbations. A new version of the plotting program in order to have outputs of more intuitive reading will be also worked out. If the debugging of the code does not become critical we should complete this level of upgrade by the end of the next reporting period.

The development of safe operating area curves will be started as planned in the statement of work. We will appreciate any suggestions from NASA/MSFC related to what is considered first priority issue.